SANDIA REPORT

SAND2007-6376
Unlimited Release
Printed October 2007

Characterizing the emissivity of materials under dynamic compression (final report for LDRD project 79877)

Daniel H. Dolan

Prepared by
Sandia National Laboratories
Albuquerque, New Mexico 87185 and Livermore, California 94550

Sandia is a multiprogram laboratory operated by Sandia Corporation,
a Lockheed Martin Company, for the United States Department of Energy's
National Nuclear Security Administration under Contract DE-AC04-94-AL85000.

Sandia National Laboratories

Issued by Sandia National Laboratories, operated for the United States Department of Energy by Sandia Corporation.

Available to DOE and DOE contractors from
U.S. Department of Energy
Office of Scientific and Technical Information
P.O. Box 62
Oak Ridge, TN 37831

Telephone: (865) 576-8401
Facsimile: (865) 576-5728
E-Mail: reports@adonis.osti.gov
Online ordering: http://www.osti.gov/bridge

Available to the public from
U.S. Department of Commerce
National Technical Information Service
5285 Port Royal Rd
Springfield, VA 22161

Telephone: (800) 553-6847
Facsimile: (703) 605-6900
E-Mail: orders@ntis.fedworld.gov
Online ordering: http://www.ntis.gov/help/ordermethods.asp?loc=7-4-0#online

SAND2007-6376
Unlimited Release
Printed October 2007

Characterizing the emissivity of materials under dynamic compression (final report for LDRD project 79877)

Daniel H. Dolan
Dynamic Material Properties
Sandia National Laboratories
P.O. Box 5800
Albuquerque, NM 87185-1181
dhdolan@sandia.gov

Abstract

Temperature measurements are crucial to equation of state development, but difficult to perform reliably. In the case of infrared pyrometry, a large uncertainty comes from the fact that sample emissivity (the deviation from a blackbody) is unknown. In this project, a method for characterizing the emissivity of shocked materials was developed. By coupling infrared radiation from the National Synchrotron Light Source to a gas gun system, broad spectrum emissivity changes were studied to a peak stress of 8 GPa. Emissivity measurements were performed on standard metals (Al, Cr, Cu, and Pt) as well as a high emissivity coating developed at Sandia.

Acknowledgments

The success of this project was the result of hard work by many different people. The construction and operation of the gas gun is due to the efforts of Jeff Gluth, Matt Gurule, Randy Hickman, Morgan Roderick, and Andrew Shay. Samples were provided by Omar Garcia, Ron Goeke, and Cathy Sobczak. Suzi Grine-Jones and Anthony Romero were responsible for target fabrication. Diagnostic support was provided by Steve Becker, Sheri Dance, Richard Hacking, Robert Malone, and Ken Moy through National Securities Technolgies and SDRD NLV-01.

Operations at the National Synchrotron Light Source resulted from the assistance of Andrew Ackerman, Larry Carr, and Chi-Chang Kao. Exxon-Mobil provided floor space on beam line U1 for the gas gun and the assistance of Andrew Mingino. Beam time on U2A and technical support from Zhenxian Liu was provided by the Carnegie DOE Alliance Center.

This work was performed under the LDRD program at Sandia National Laboratories (project 79877). Sandia is a multiprogram laboratory operated by Sandia Corporation, a Lockheed Martin Company, for the United States Department of Energy's National Nuclear Security Administration under Contract DE-AC04-94AL85000.

Table of Contents

List of Figures

List of Tables

CHAPTER 1
Introduction

Mechanical diagnostics (*e.g.*, VISAR [1]) provides a wealth of mechanical information about materials under dynamic compression, but this information is incomplete without knowledge of the temperature. For example, a material's pressure-temperature phase diagram can only be inferred from mechanical measurements through comparisons with existing equations of state. Temperature is difficult to measure because of the short time scales ($< 10^{-6}$ seconds) and extreme conditions in dynamic compression experiments, which are incompatible with common temperature diagnostics.

Infrared pyrometry is a potentially useful method for determining the temperature of a dynamically compressed sample. This method relies on the principle that an object emits radiation that scales with temperature in a known manner. A key difficulty in using pyrometry is that this scaling is not always known for real objects, particularly under compression.

1.1 Project purpose and scope

The purpose of this project is to investigate the emissivity of materials under dynamic compression conditions. Emissivity describes the way in which a real sample's emission deviates from an ideal sample (a blackbody). This deviation may change as the sample moves away from the ambient state.

The spectral range of interest in this work is the near-infrared to mid-infared, roughly 1000-5000 nm. This range corresponds to temperatures of 600–2900 K (for peak blackbody emission), and spans conditions in isentropic and shock wave compression experiments. Longer wavelengths are potentially of interest at lower temperatures, but are difficult to probe due to the absorption edge of relevant window materials (lithium fluoride and sapphire).

The approach of this project is to interface a gas gun to a synchrotron source for time-resolved infrared reflectance measurements of shocked materials. Synchrotron radiation is widely used in static compression research, but rarely in real-time, single-event measurements. Synchrotrons produce extremely bright emission that spans the infrared, visible, ultraviolet, and x-ray spectrum. Although higher energy applications are beyond the

immediate scope of this project, the successful shock wave experiments at a synchrotron provides a path to future x-ray applications.

1.2 Chapter organization

Background information relevant to this project is presented in Chapter 2. The experimental methods used are described in Chapter 3. Chapter 4 summarizes the results of three experimental campaigns performed during this project, the results of which are analyzed in Chapter 5. A project summary and suggestions for future work are given in Chapter 6.

CHAPTER 2

Background

A fundamental challenge in pyrometry measurements is transforming radiance measurements to sample temperature. For an ideal object, known as a blackbody, this conversion is exact. However, real samples deviate from blackbody emission, and additional information is needed to infer the proper temperature.

This chapter presents background information relevant to the shortcomings of pyrometry measurements. First, a brief review of blackbody radiation is given. Next, the difficulties of emissivity are described, along with the potential solution—emissivity standards. Finally, technical challenges for the project are summarized.

2.1 Blackbody emission

For an ideal blackbody, the relationship between spectral radiance L (power per unit area per unit solid angle per unit wavelength), temperature T, and wavelength λ is given by Plank's law [2]:

$$L(\lambda, T) = \frac{2hc_0^2}{\lambda^5 \left(e^{hc_0/\lambda kT} - 1\right)} \tag{2.1}$$

where c_0 is the speed of light and h is Plank's constant. Figure 2.1 shows blackbody emission curves at several different temperatures. As temperature increases, the emission curve increases overall (meaning more light is radiated) and the peak of the curve moves to shorter wavelengths. The product of temperature and peak emission wavelength equals a constant value, 2897.7 μm·K.

Given one or more measurements of an object's radiance, it is (in principle) straightforward to determine the object's temperature. The process is simplest for measurements in a narrow spectral region, but can also be applied to a well defined band. In many circumstances, it is useful to use Wien's law [3].

$$L(\lambda, T) \approx \frac{2hc_0^2}{\lambda^5} e^{-hc_0/\lambda kT} \tag{2.2}$$

a useful approximation for measurements on the short wavelength side of the blackbody peak.

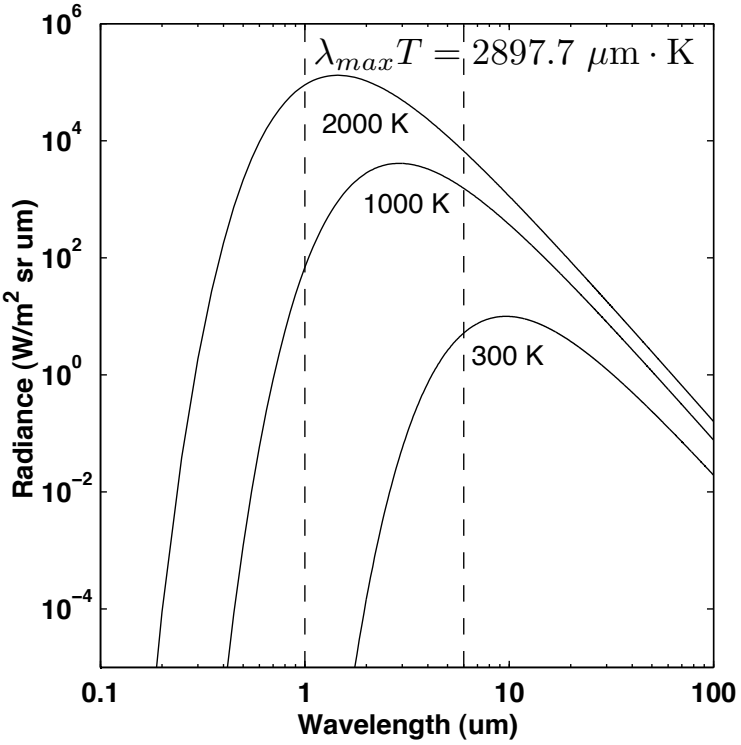

Figure 2.1. Blackbody emission as a function of wavelength at various temperatures

2.2 The emissivity problem

A blackbody must absorb all radiation that falls upon it—none of this radiation must pass through or be reflected from the object. The condition is never met exactly, so there are no true blackbodies.

The radiance generated by a real object can scaled with respect to a blackbody at the same temperature using a parameter known as the emissivity (ε).

$$L(\lambda, T) = \varepsilon \left(\frac{2hc_0^2}{\lambda^5 \left(e^{hc_0/\lambda kT} - 1 \right)} \right) \tag{2.3}$$

Emissivity is bounded between zero (a perfect reflector or transparent object) and unity (a perfect blackbody). In thermodynamic equilibrium, emissivity must equal absorption [3], and can be therefore tied to an object's reflectivity (ρ) and transmission (τ).

$$\varepsilon(\theta) = 1 - \rho(\theta; 2\pi) - \tau(\theta; 2\pi) \tag{2.4}$$

Emissivity is a directional quantity, describing emission from a surface viewed at an angle θ from the normal.[1] Reflectivity and transmission are directional-hemispherical quantities, and describe the reflection/transmission of incident radiation in a particular direction to the appropriate half space.

Without knowledge of an object's emissivity, it is impossible to unambiguously calculate temperature in a pyrometry measurement. A lower temperature estimate can be obtained by assuming the object is a blackbody, but this is a poor estimate for highly reflective materials (such as metals). In some situations, objects are assumed to be gray bodies, which is to say that the emissivity is wavelength independent; given two or more closely spaced radiance measurements, one can calculate temperature with some confidence. However, emissivity is generally a function of wavelength, and ignoring this variation can be treacherous. Using Wien's law (Equation 2.2), one can show that temperature uncertainty scales with emissivity uncertainty for a given radiance.

$$\frac{\Delta T}{T} \approx \frac{\lambda kT}{hc_0} \frac{\Delta \varepsilon}{\varepsilon} \tag{2.5}$$

2.2.1 Causes of emissivity change

For opaque objects, ambient emissivity values are readily determined from reflectivity measurements or optical constant data [4]. What is not known, however, is how emissivity changes when an object is subject to conditions very different from the ambient state. Dynamic compression is an extreme case where emissivity changes are a concern in pyrometry measurements. Moving from ambient pressure to much higher stresses (0.1–100 GPa) can dramatically alter the emissivity of a sample, whether due to the compression itself or

[1] Azimuthal symmetry is assumed throughout this discussion.

the corresponding temperature change in the (typically) adiabatic process. Discontinuous emissivity changes are also to be expected if the object undergoes a phase transition during compression. Reflectance geometry is another concern as an initially specular sample might become diffuse during compression.

2.2.2 Dealing with emissivity change

Several approaches have been used for dealing with emissivity change in shocked samples. The simplest method is to assume extremely conservative bounds to the emissivity [5]; this approach is aided by the use of short wavelength channels, which are less impacted by emissivity for a given signal-noise level (Equation 2.5). Combined reflectance and pyrometry approaches can be used to probe the emissivity of compressed samples, but these methods are not ideal ideal. Attaching an integrating sphere to a sample provides a measure of total hemispherical reflectivity during compression [6], but the method is potentially difficult and expensive proposition. Other reflectance approaches [7] work well in some circumstances, but require assumptions about the surface under which may not be valid in general.

The purpose of this project is to develop emissivity standards, which once characterized can be used in any pyrometry measurement. The idea is that rather than dealing with the emissivity of any given material, one could build up a suite of standard materials for which the emissivity is known (or at least well bounded) over a wide range of conditions. For a material to function as an emissivity standard, it must be readily applied to many substrate materials, sufficiently opaque to screen radiation from the substrate, and relatively thin to allow rapid thermal equilibrium with the substrate. Ideally, the standard should also mimic a blackbody as closely as possible, both to increase the signal levels and to strongly constrain the temperature calculation. Since emissivity can never exceed unity, emissivity standards close to unity have very little room for upward variation. An important specification is that the standard's emissivity not decrease (either by becoming more transparent or reflective) when exposed to extreme conditions.

Essentially, the emissivity standard described above must be non-reflective, opaque, and very thin (< 1000 nm). Achieving all three specifications simultaneously is not an easy task. Metals, which are opaque in the specified thickness range, are highly reflective. Dielectrics, which can be minimally reflective, must typically be much thicker than 1000 nm to achieve opacity. Manufacturing a high emissivity coating is not a great challenge—many commercial paints and other processes readily do the trick in both the visible and infrared spectrum. Making a *thin* high emissivity coating (particularly one that can withstand extreme conditions) is challenging, but some progress has been made. A process discovered at Sandia (disclosure #10260) achieves many of these goals.

Figure 2.2 shows an example of the Sandia high emissivity coating (typical thickness 300 nm) applied to a diamond turned (DT) copper substrate. Like all metals, copper is very good reflector in the infrared ($> 90\%$), and is thus a poor emitter. After the application of the coating, sample emissivity increases to more than 50% across the mid-infrared spec-

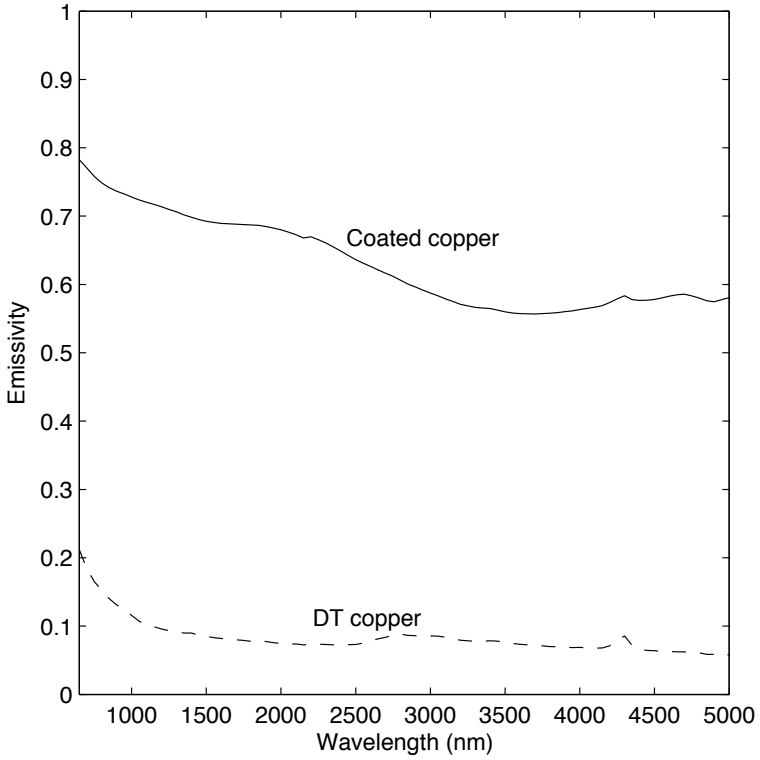

Figure 2.2. Example of a high emissivity standard film.

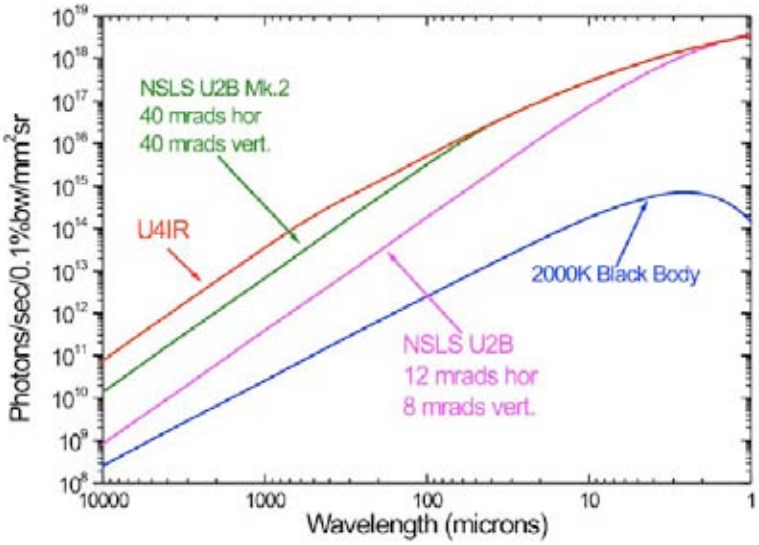

Figure 2.3. Emission profile of the NSLS VUV ring

trum. For a given temperature, the coated sample would emit substantially more light than the uncoated sample, and the associated temperature uncertainty in a pyrometry measurement should be substantially reduced, assuming that emissivity does not decrease from its ambient value. Furthermore, combining the high emissivity coating with a self-irradiating geometry (see Chapter 10 of Reference 3) could readily boost the apparent emissivity near unity.

2.3 Technical challenges

A bright radiation source is needed to characterize infrared emissivity via reflectance measurements (Equation 2.4) within the short duration of a dynamic compression experiment. The National Synchrotron Light Source (NSLS) was selected for this project for several reasons. First, emission by the vacuum-ultraviolet (VUV) ring is orders of magnitude brighter than conventional infrared sources, such as blackbodies (Figure 2.3). Unlike laser sources, the synchrotron emits all wavelengths simultaneously, allowing reflectance measurements to mimic broad spectrum pyrometry. Synchrotron emission is nearly diffraction limited, allowing illumination to be tightly confined within a narrow angular and/or spatial domain. Unlike blackbody radiation, synchrotron radiation is pulsed: on the VUV ring, 1-2 ns emissions occur every 18.9 ns (seven pulses, followed by two gaps).

Although synchrotron radiation is widely used in static compression research, this project represents its first application to dynamic compression. Several issues need to be addressed to make such measurements possible, such as:

- Real-time, single-event operation

Most NSLS applications are essentially static, which is to say that the measurement is performed over many, many synchrotron orbits. For this project, the reflectance measurement needed to be made within only a few orbits.

- Safety
  Although dynamic compression experiments are common with the NNSA laboratories, these experiments were new to the NSLS at the start of this project. Significant safety reviews were needed before experiments could begin.

As described in the following chapters, these challenges were successfully met, initiating a new class of research for Sandia and Brookhaven National Laboratories.

CHAPTER 3

Experimental methods

This chapter summarizes dynamic reflectance measurements performed at the NSLS. First, a description of the impact experiment is given. Next, an outline of the infrared reflectance measurements is presented. Throughout this chapter, discussion is fairly general as the experimental methods evolved during the project. Specific experimental details for each campaign may be found in the next chapter.

3.1 Impact experiments

Plate impact was used to produce one dimensional strain in various sample materials [8]. The technique uses inertial confinement to create a state of uniaxial strain for a brief period of time (1000 ns, in this case). Experiments were performed using a light gas gun in a symmetric impact configuration as described below.

3.1.1 NSLS gas gun system

Figure 3.1 shows the single-stage gas gun constructed for this project. This gun is based on a design from Washington State University with modifications by National Security Technologies; the system used at NSLS is identical to a gas gun operated at the Sandia DICE facility. The gun uses a wrap around [9] breech (1000 psi max pressure) to accelerate 3" diameter aluminum projectiles through the barrel and into the target chamber. In each experiment, a target is mounted in the chamber to achieve near-normal (within a few milliradians) impact.

The gas gun was constructed within a shipping container in the summer of 2006. After a series of validation shots to verify safe operation and velocity/tilt performance, the container was shipped to Brookhaven National Laboratories (August 2006). Figure 3.2 shows the initial installation of the Sandia gas gun at NSLS. The gun rail was installed on a portion of the U1 beam line of the VUV ring. Infrared light was extracted from the ring at beam line U2A directed to the gun with a series of turning mirrors.

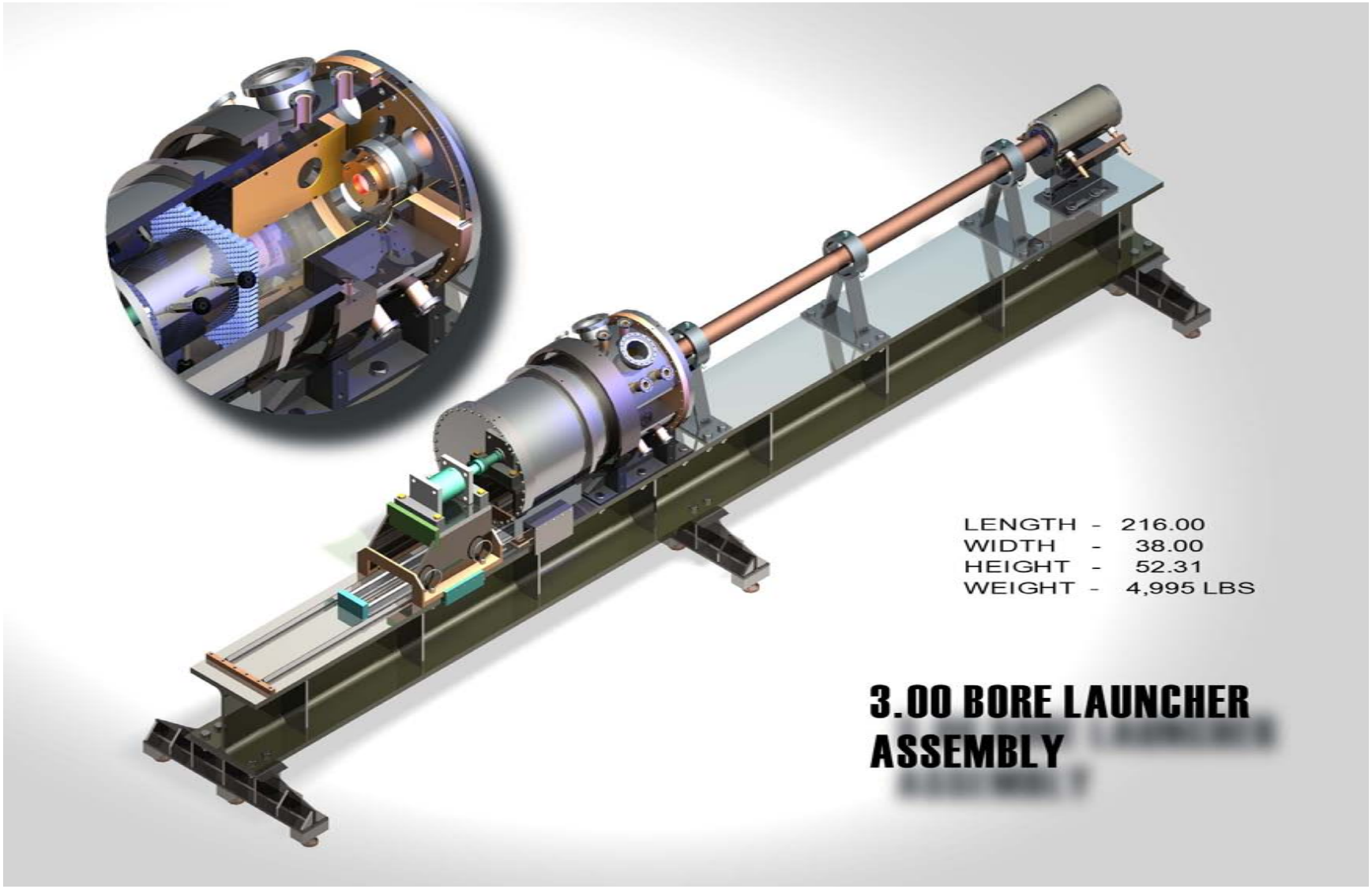

Figure 3.1. The 3" gas gun. Compressed helium drives projectiles from the breech (right end) to the target chamber (left end).

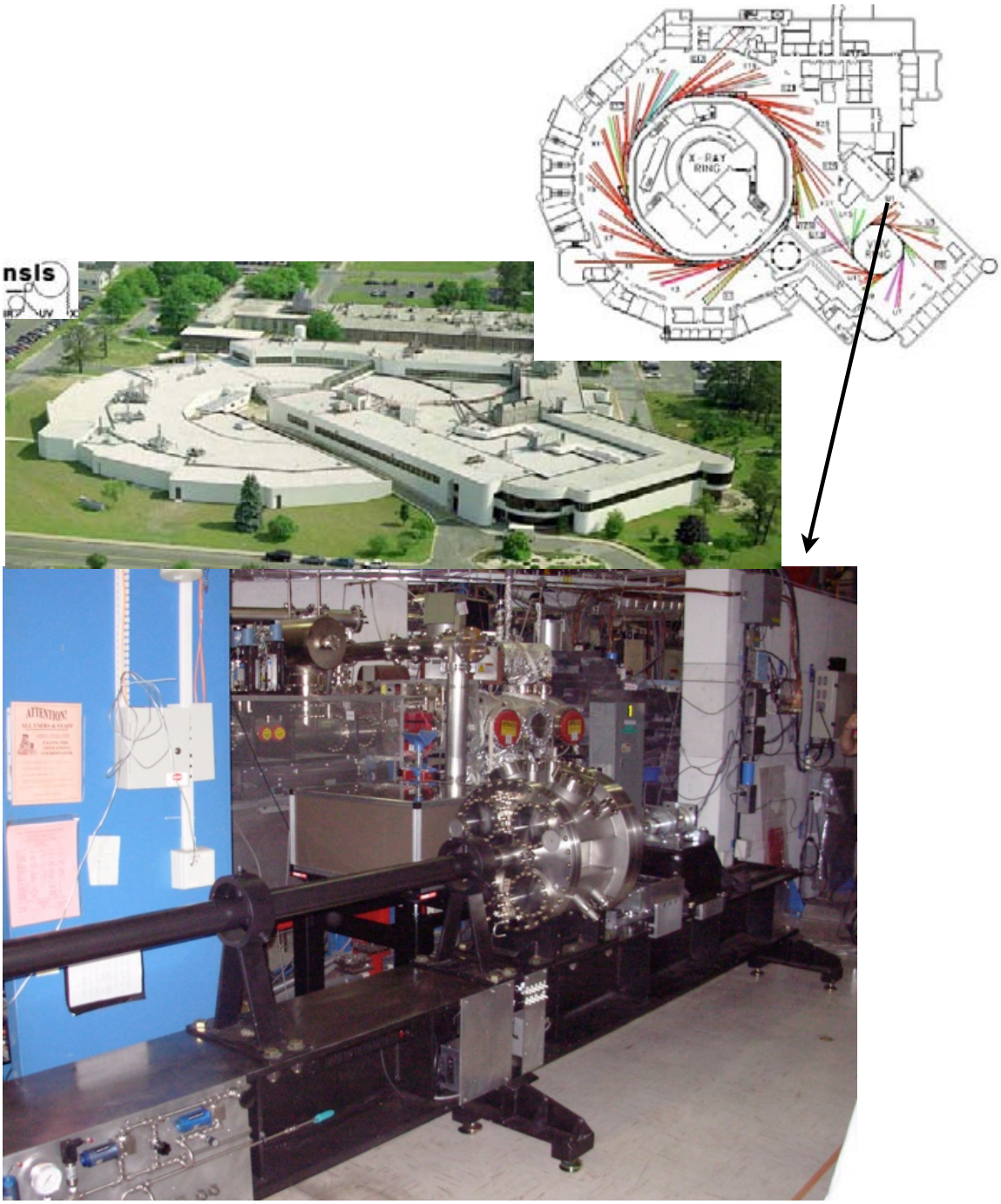

Figure 3.2. Sandia gas gun at the NSLS

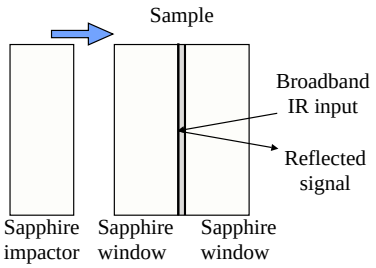

Figure 3.3. Symmetric impact configuration

3.1.2 Symmetric impact configuration

Figure 3.3 shows the symmetric impact configuration used throughout this work. The use of sapphire as both an impactor and window material is important for several reasons:

- Symmetry
  The impact symmetry in Figure 3.3 imposes a useful constraint on the peak state—the particle velocity in this state must equal half of the impact velocity.
- Mechanical properties
  The mechanical response of sapphire is well known, and the material is known to be elastic and transparent beyond 10 GPa [10]. Furthermore, the relatively large mechanical impedance of sapphire allows moderate stresses to be generated at modest impact velocities.
- Other properties
  Sapphire is transparent to at least 4500 nm, allowing study in the visible, near-infrared, and mid-infrared spectrum. Also, sapphire is minimally heated under elastic shock compression, and readily conducts heat from the thin sample because of its large thermal conductivity. Hence, the sample temperature can effectively be controlled independently of the stress state.

All experiments in this project were constructed from a-axis HEMEX sapphire. The front and rear windows were bonded together with either AngstromBond 9110LV (a standard epoxy at Z) or Loctite 326 (a favored glue in pyrometry research [11]). Samples in this project were fabricated by electron-beam assisted physical vapor deposition and sputtering techniques. Vapor deposition samples were provided by the KTech Materials Processing and Coatings Laboratory (MPCL); sputtered samples were provided by the Thin Film, Vacuum & Packaging department (Sandia organization 2452). Samples were located in one of three locations as illustrated in Figure 3.4. In standard reflectance measurements,[1]

[1]The term "standard" is used because this configuration mimics pyrometry targets at Sandia and Los Alamos National Laboratories. The reverse configuration is reminiscent of a pyrometry configuration used at Lawrence Livermore National Laboratory [12].

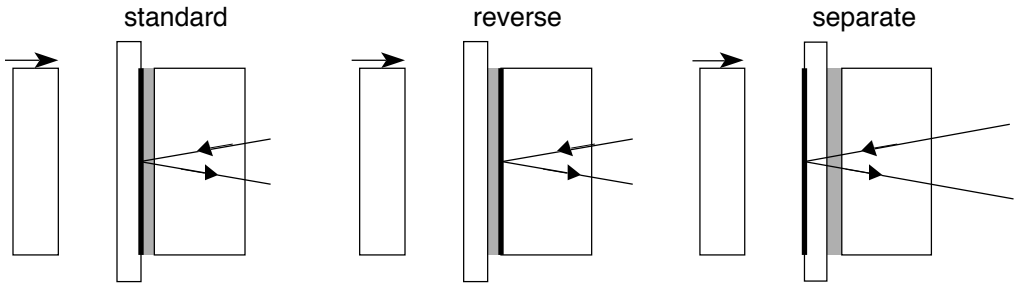

Figure 3.4. Sample locations in a symmetric impact experiment

the sample is deposited on the interior surface of the front sapphire window; light passes through the bond holding the front and rear windows together during the measurement. Reverse reflectance measurements have the reflective sample deposited on the interior rear window surface so light does not pass through the glue during the measurement. Separate reflectance measurements (used primarily for diagnostic purposes) have the sample at the impact surface, not in contact with the front window/rear window bond. Light passes through the bond in the separate configuration, but the bond is compressed at different time than the film.

3.2 Dynamic reflectance measurements

The focus of this project was on specular reflectance changes, since the materials under study are specular films deposited on a highly polished sapphire substrate. As such, optical relays used in this project were designed to couple light from the VUV ring (which is roughly collimated) to the sample in a near-normal fashion (with a small angular illumination range) and collect the specularly reflected light. A series of band pass filters [13] was used to separate light reflected by the target into 3–4 spectral bands, which were recorded by several fast infrared detectors. Gold coated mirrors and sapphire windows were used throughout the optical system, limiting measurements to wavelengths of 800–4500 nm.

Standard Si (Thorlabs DET210) and InGaAs (Thorlabs DET410) photodiodes were used for near-infrared measurements below 2000 nm. Attempts to use HgCdTe photodiodes (LN cooled Kolmar detectors) proved fruitless as the preamplifier recovery time exceeded the pulse-pulse time of the synchrotron. In their place, HgCdTe photoelectromagnetic (PEM) detectors [14] were used to record mid-infrared radiation.

CHAPTER 4

Experimental results

This chapter presents the results of three experimental campaigns performed at NSLS. For clarity, each section describes a specific campaign, during which consistent target fabrication, optical relays, and diagnostic systems were used. Specific experimental layouts, which evolved from one campaign to the next, are described in each section.

4.1 Campaign I (September 2006)

The first NSLS campaign took place September 11–18, 2006. Figure 4.1 shows the optical layout used in this campaign. Collimated synchrotron light was reduced by a pair of off-axis parabolic mirrors and sent through a sapphire port into the target chamber. This light was focused onto the sample with third parabolic mirror, which also collected the reflected light. The return light was sent through the same optical port to the dichroic beamsplitters and infrared detectors. The first beam splitter in the system reflected light between 1100 and 2800 nm; this light was collected by an InGaAs detector (1100–1800 nm sensitivity), yielding a 1100–1800 nm channel. Light passing through the first beam splitter encountered a second beam splitter, which reflected light between 3100 and 3900 nm. The output of this beam splitter was recorded by two PEM detectors. The first channel (PEM1) measured 3100–3900 nm, and the second channel (PEM2) measured 2800–3100 nm and 3900–4500 nm. The strange band combination on the second PEM detector stemmed from a design oversight that was corrected in the next campaign. An InGaAs monitor photodiode was placed upstream of the gas gun to track synchrotron variations.

Figure 4.2 shows the diagnostic timing approach used during the September 2006 campaign. A series of shorting pins mounted within the target plate ("G" for ground, "L" for long, "M" for medium, and "S" for short) were positioned at roughly 2 mm intervals; the projectile strike on these pins generated a series of pulses from which the impact velocity was determined. The short pin pulse was used to activate the velocity digitizer and a delay generator. Output from the delay generator was used to activate the diagnostic and impact tilt digitizers. Since the VUV ring undergoes several orbits during the plate impact experiment, precise synchronization between impact and the emitted light pulses was not required. Instead, a wide digitizer window and 50% pre-trigger interval was used to ensure that the impact event was recorded.

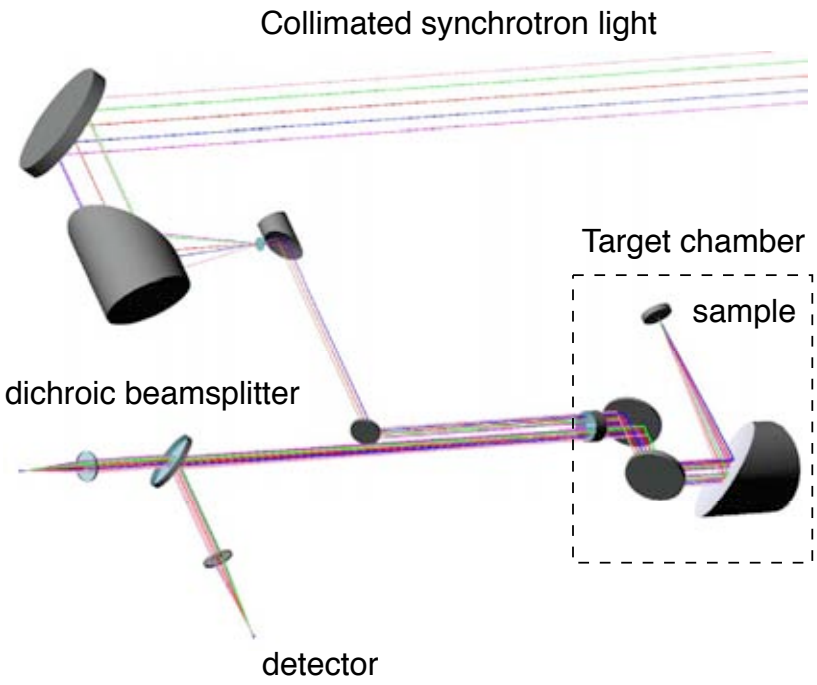

Figure 4.1. Optical relay A

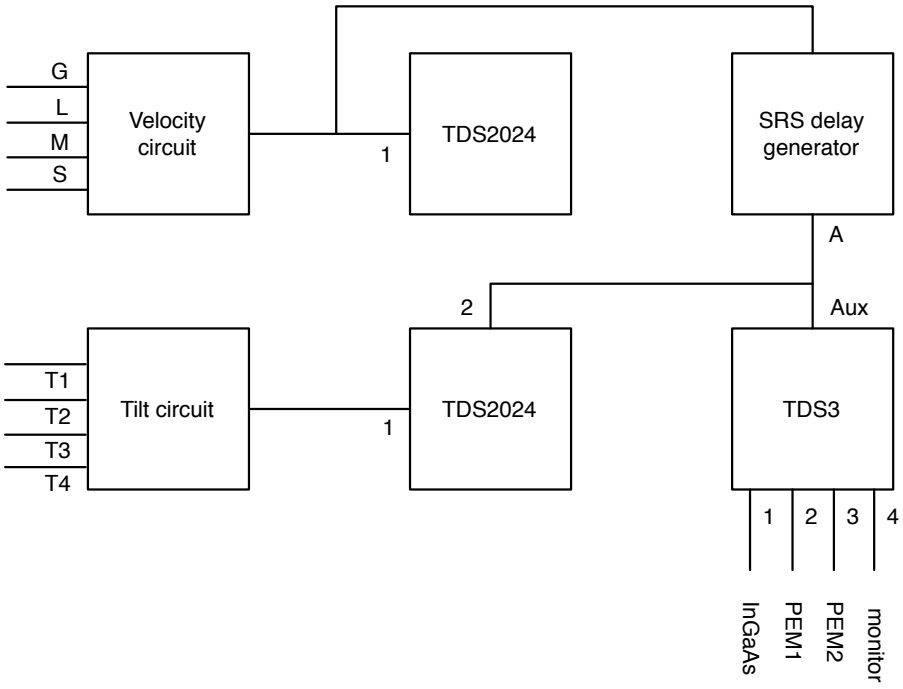

Figure 4.2. Timing setup for September 2006 experiments

Table 4.1. NSLS campaign I summary. All samples in this campaign were fabricated by MCPL.

ID	configuration	sample	bond	v_{imp} (m/s)
NSLS06-14	standard	Al	AngstromBond	371
NSLS06-21	standard	Al	AngstromBond	360
NSLS06-18	standard	Cr	AngstromBond	361
NSLS06-20	standard	Cr	AngstromBond	362
NSLS06-19	standard	Cu	AngstromBond	362
NSLS06-15	standard	high ε	AngstromBond	364
NSLS06-22	standard	high ε	AngstromBond	350
NSLS06-17	standard	high ε	AngstromBond	221

The nine experiments performed during the first NSLS experiment campaign are summarized in Table 4.1. All experiments used the standard configuration, with AngstromBond holding the front and rear windows of the target stack together. All coatings were deposited at the Materials Processing and Coatings Laboratory (MPCL).

4.1.1 Aluminum experiments

Two aluminum experiments—NSLS06-14 and NSLS06-21—were performed at 8 GPa. The results are shown in Figures 4.3 and 4.4. In NSLS06-14, no apparent change in reflectivity was noted in the near-infrared; a minor increase may have occurred on the first PEM channel. By comparison, a clear decrease in sample reflectivity was observed in NSLS06-21 across all channels.

4.1.2 Chromium experiments

Two chromium experiments—NSLS06-18 and NSLS06-20—were performed at 8 GPa. The results are shown in Figure 4.5 and Figure 4.6. Both experiments showed a drop in the near-infrared reflectance, with what appears to be a minor increase in reflectance in the first PEM and inconsistent results in the second PEM.

4.1.3 Copper experiment

One copper experiment—NSLS06-20—was performed to a peak pressure of 8 GPa. The results are shown in Figure 4.7. A clear loss of reflected signal was observed on all three channels.

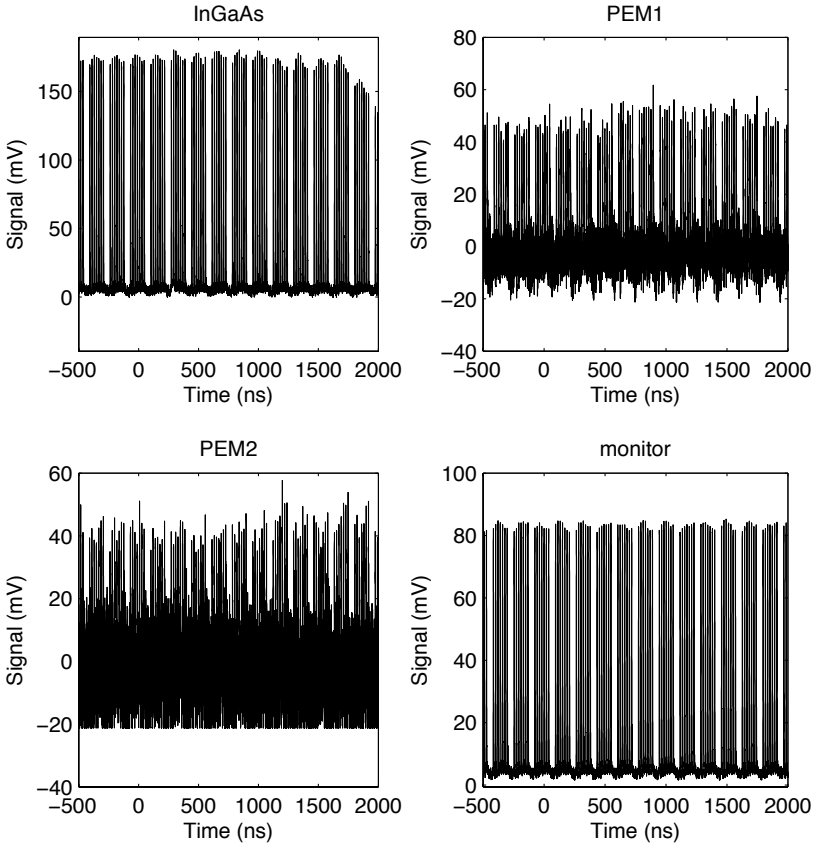

Figure 4.3. Raw signal data from NSLS06-14 (Al compressed to 8 GPa)

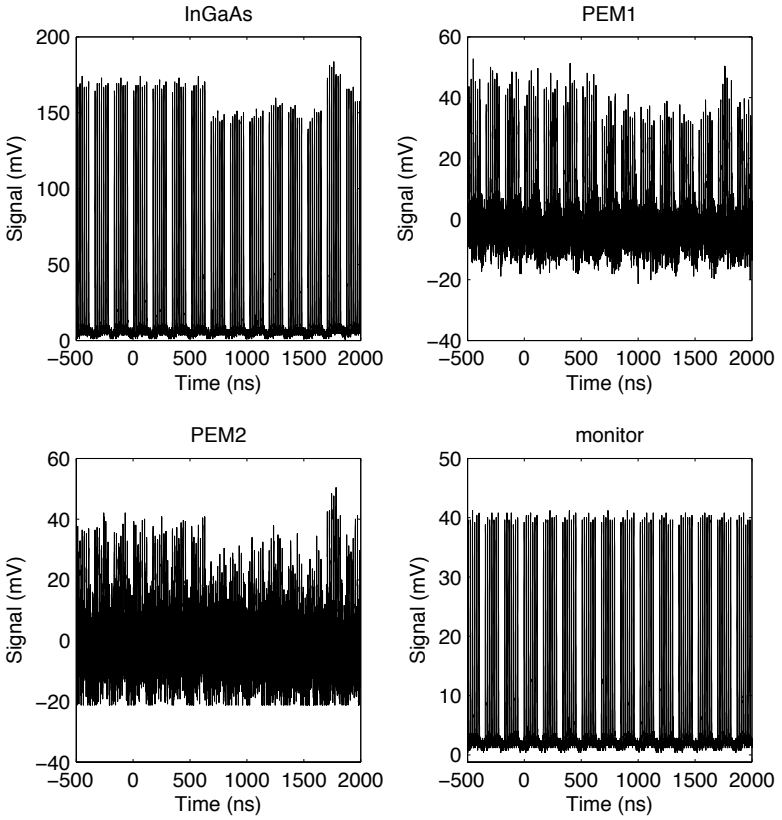

Figure 4.4. Raw signal data from NSLS06-21 (Al compressed to 8 GPa)

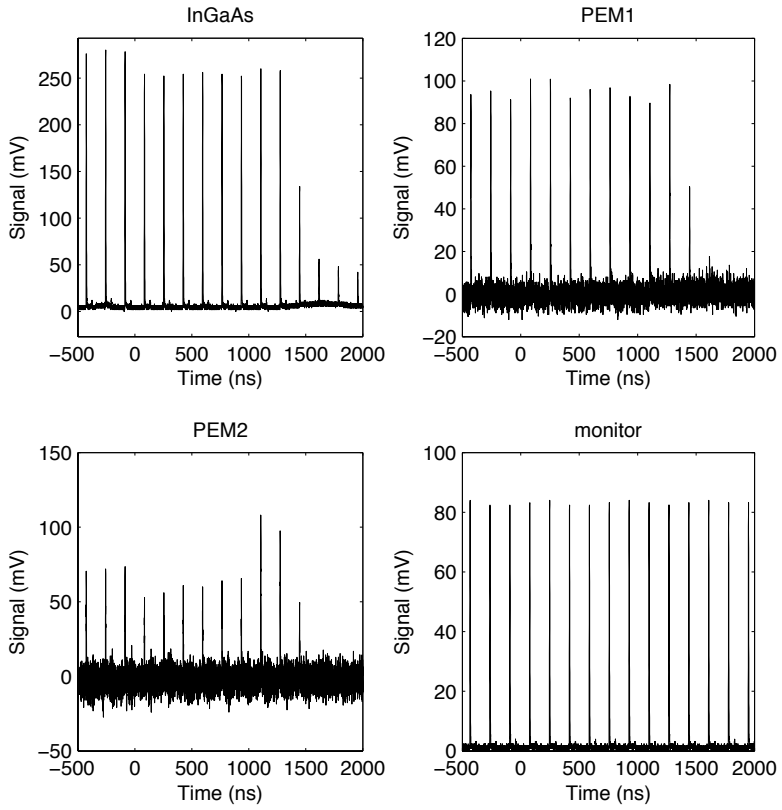

Figure 4.5. Raw signal data from NSLS06-18 (Cr compressed to 8 GPa)

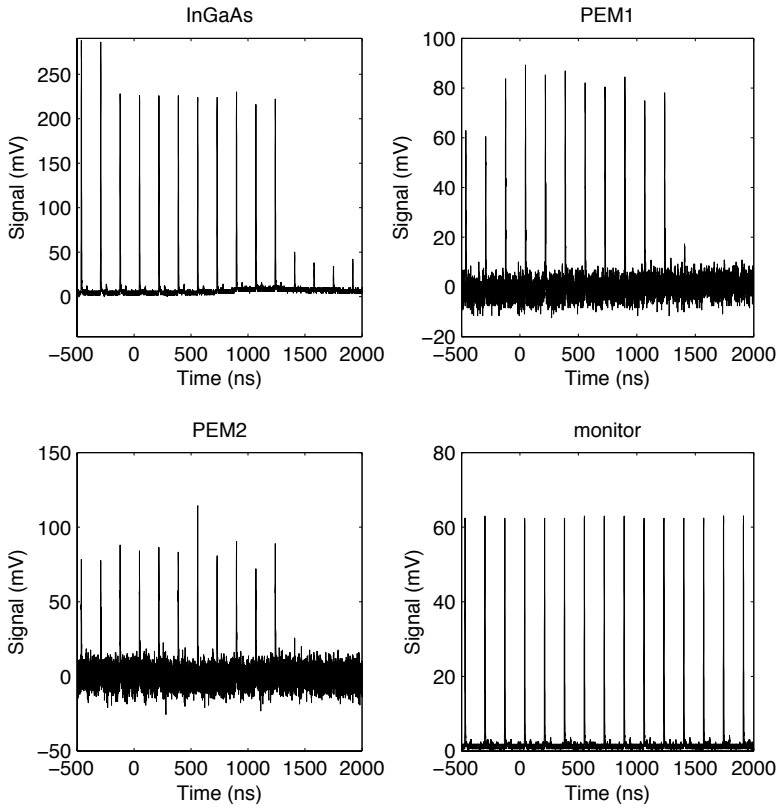

Figure 4.6. Raw signal data from NSLS06-20 (Cr compressed to 8 GPa)

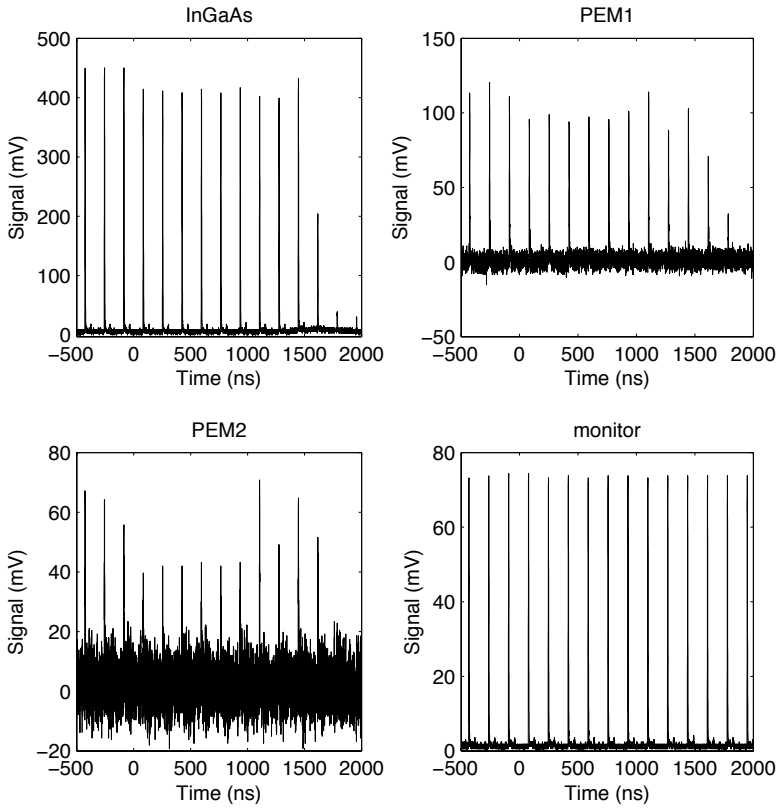

Figure 4.7. Raw signal data from NSLS06-19 (Cu compressed to 8 GPa)

4.1.4 High emissivity film experiments

Two high emissivity film experiments—NSLS06-15 and NSLS06-22—were performed at 8 GPa. The results are shown in Figures 4.8 and 4.9. Unlike other experiments in the campaign, an impact flash was observed (more so in NSLS06-15 than in NSLS06-22). A clear loss of reflected signal was observed for the near infrared in both experiments. The mid-infrared channels are less definitive. The first PEM showed a signal gain in NSLS06-15 but a decrease in NSLS06-22. The second PEM showed a minor increase in NSLS06-16 and no obvious change in the NSLS06-22.

One high emissivity experiment—NSLS06-17—was performed at 5 GPa. The results are shown in Figure 4.10. Unlike the higher pressure experiments on this film, no impact flash was detected. A clear loss of near-infrared signal was observed. The first PEM channel failed during the shot, and no data was obtained. The second PEM channel suggests a minor increase in reflected light.

4.2 Campaign II (April 2007)

The second NSLS campaign took place April 18–27, 2007. To simplify construction and alignment of the optical setup, a revised reflectance configuration (Figure 4.11) was designed. In this configuration, an obtuse prism directs light input from one optical port to the sample and sends the reflected light to a second optical port. The beam splitter and detector configuration was also changed. The first beam splitter now reflected 800–900 nm light, which was recorded by a Si photodiode. The next beam splitter reflected light between 1100–2800 nm; light passing through this splitter was recorded by a PEM detector (covering 2800-4500 nm). Light reflected by the second beam splitter went to a third beam splitter which reflected light between 1100 and 1500 nm. Reflected light went to an InGaAs photodiode (measuring 1100–1500 nm), while transmitted light went to a PEM detector (1500-2800 nm). To reduce electromagnetic noise effects, all output detectors were placed in a steel Hoffman box.

To accomodate the Si detector, a second digitizer was added as shown in the revised timing configuration (Figure 4.12). A clock pulse from the VUV ring was also recorded for diagnostic purposes.

Experiments performed during this campaign are summarized in Table 4.2. A variety of target materials (all fabricated by organization 2452) and configurations were tested during the campaign.

4.2.1 Aluminum experiments

Two standard aluminum experiments—NSLS07-11 and NSLS07-12—were performed near 8 GPa. The results are shown in Figures 4.13 and 4.14. Consistent loss of reflected light was observed in both experiments. At near visible wavelengths, the loss is substantial,

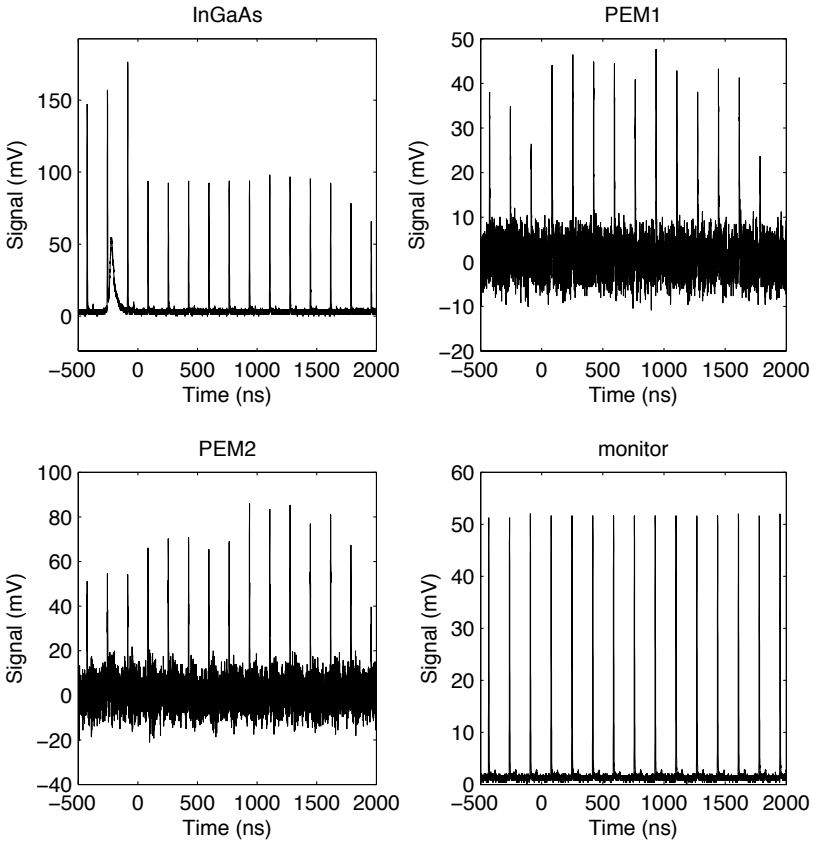

Figure 4.8. Raw signal data from NSLS06-15 (high emissivity film compressed to 8 GPa)

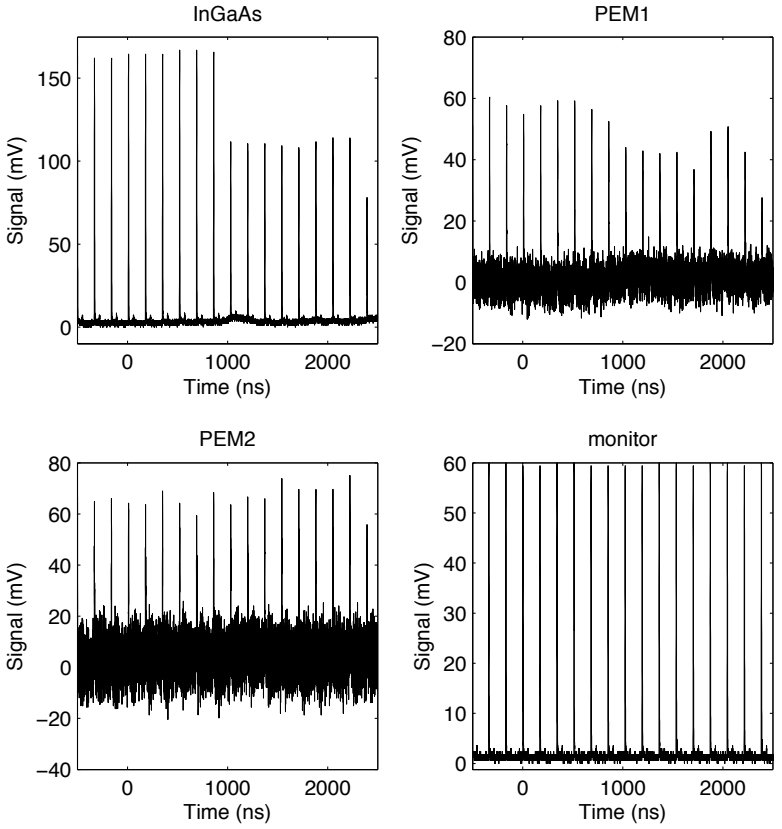

Figure 4.9. Raw signal data from NSLS06-22 (high emissivity film compressed to 8 GPa)

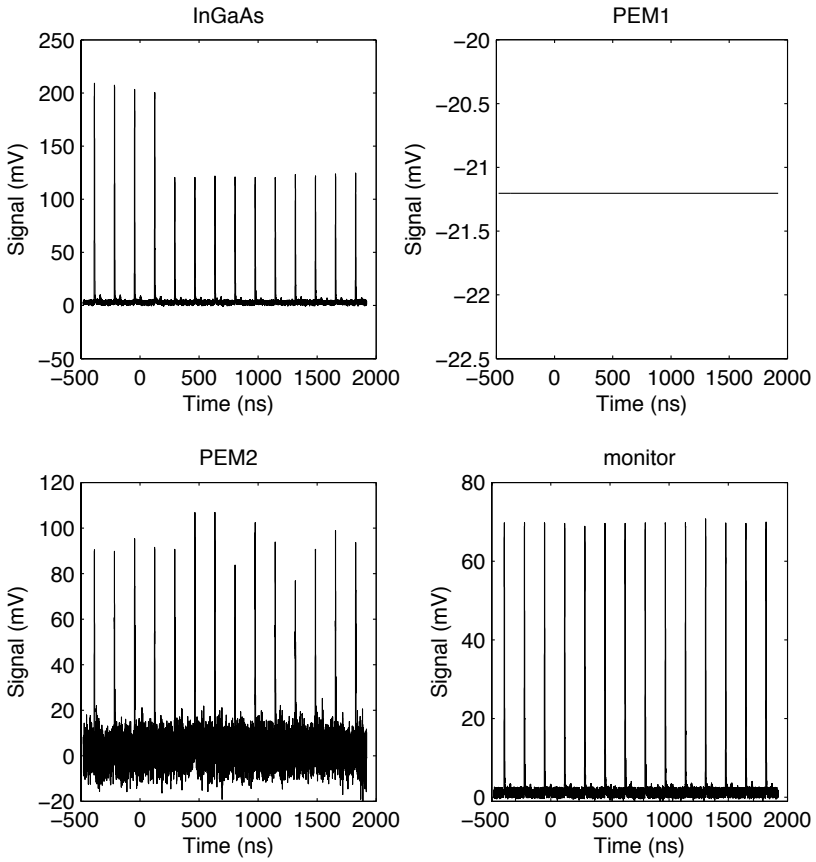

Figure 4.10. Raw signal data from NSLS06-17 (high emissivity film compressed to 5 GPa)

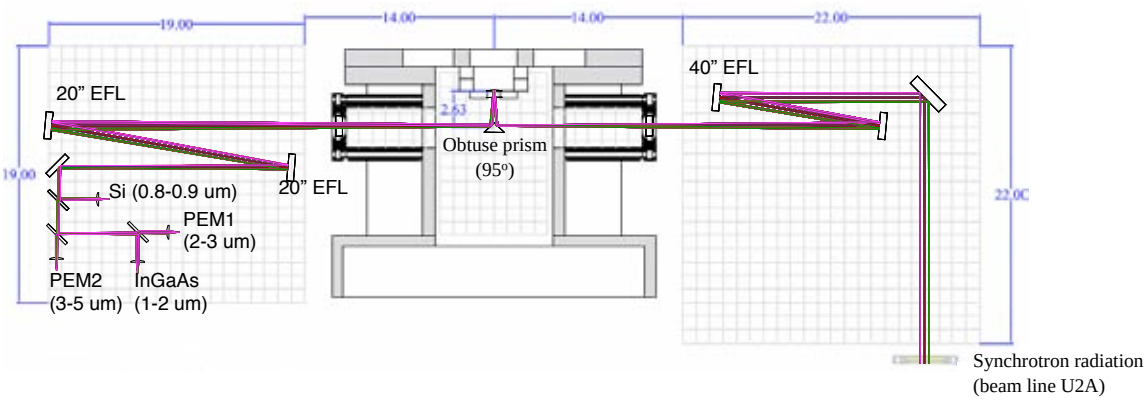

Figure 4.11. Optical relay B

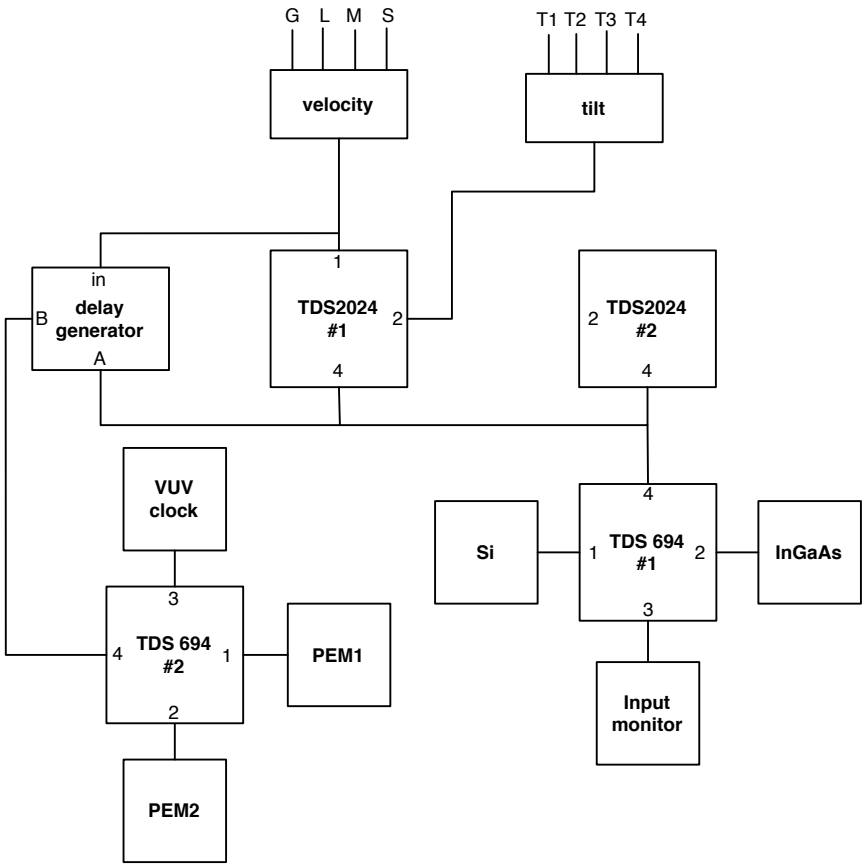

Figure 4.12. Timing setup for April 2007 experiments

Table 4.2. NSLS campaign II summary. All samples were fabricated by organization 2452.

ID	configuration	sample	bond	v_{imp} (m/s)
NSLS07-11	standard	Al	AngstromBond	367
NSLS07-12	standard	Al	Loctite 326	376
NSLS07-13	reverse	Al	AngstromBond	378
NSLS07-14	reverse	Al	Loctite 326	382
NSLS07-15	separate	Al	AngstromBond	377
NSLS07-06	reverse	Cr	AngstromBond	369
NSLS07-19	reverse	Cr	AngstromBond	378
NSLS07-17	reverse	Cu	AngstromBond	371
NSLS07-18	reverse	Cu	AngstromBond	374
NSLS07-07	reverse	Pt	AngstromBond	378
NSLS07-20	reverse	Pt	AngstromBond	380
NSLS07-21	reverse	Pt	AngstromBond	372
NSLS07-09	standard	high ε	AngstromBond	230
NSLS07-10	standard	high ε	AngstromBond	230
NSLS07-05	standard	high ε	AngstromBond	369
NSLS07-08	standard	high ε	AngstromBond	374

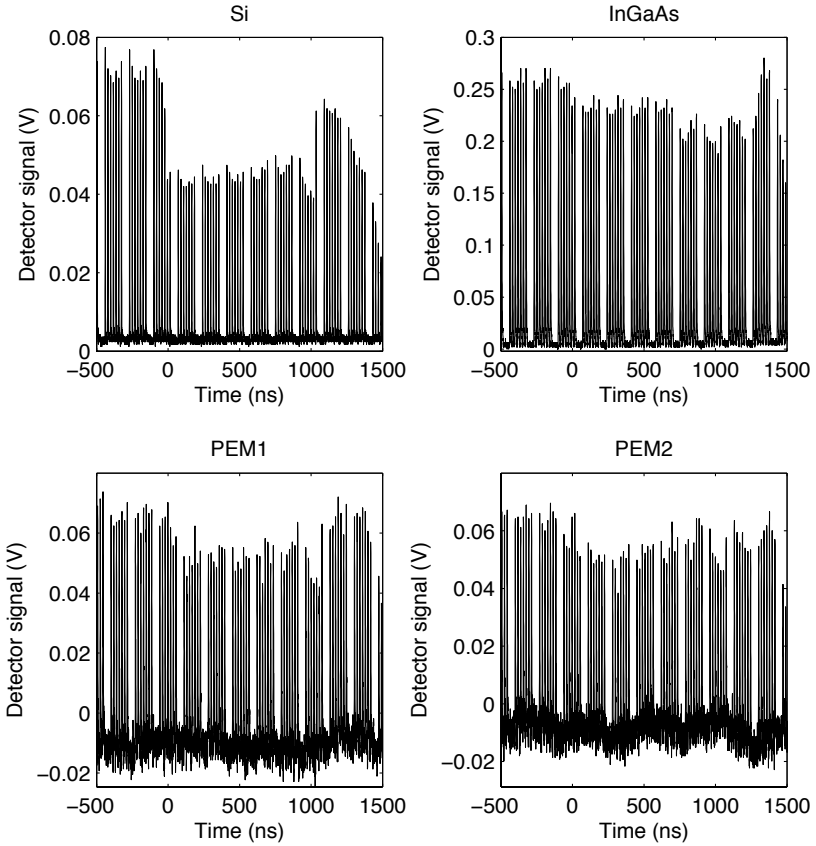

Figure 4.13. Raw signal data from NSLS07-11 (standard Al at 8 GPa)

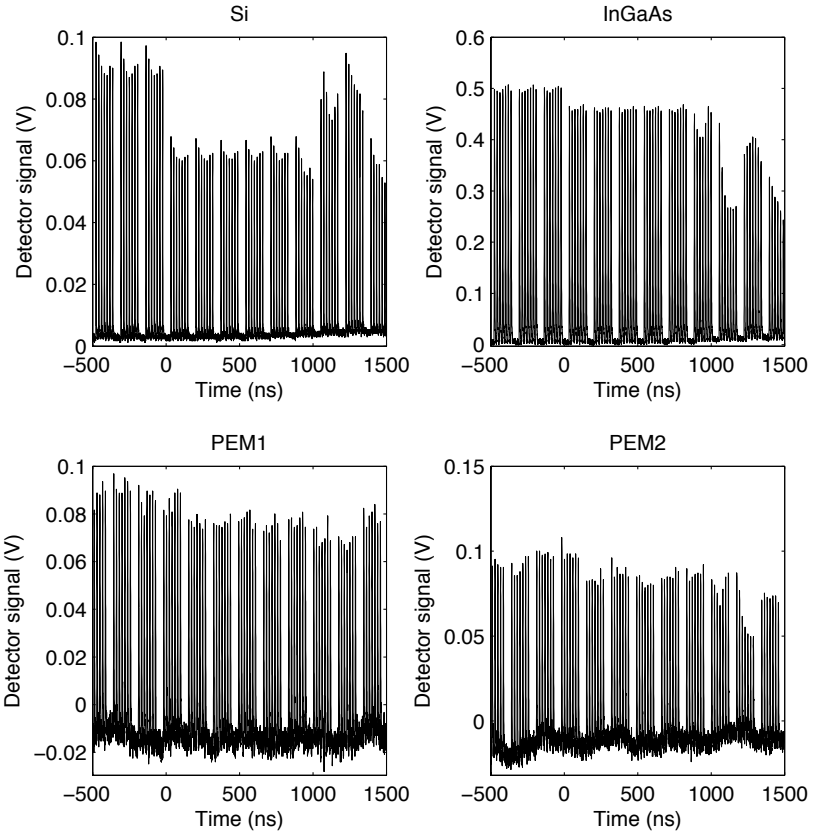

Figure 4.14. Raw signal data from NSLS07-12 (standard Al at 8 GPa)

while losses at 1000–1800 nm are minimal. Increased loss was observed at mid-infrared wavelengths, though not nearly as much as in the near visible domain.

Two reverse aluminum experiments, NSLS07-13 and NSLS07-14, were also performed at 8 GPa. The results are shown in Figures 4.15 and 4.16. Very different behavior was observed in these experiments. Although light did *not* pass through a bond layer, substantial loss in apparent reflectance was observed in NSLS07-13, while no real changes were observed in NSLS07-14.

A single separate configuration aluminum experiment, NSLS07-15, was performed at 8 GPa. The results are shown in Figure 4.17. An immense impact flash[1] was observed on all detector channels. The long duration of this flash overlaps with shock compression of the epoxy layer, making it difficult to assess the apparent reflection drop after the epoxy layer is compressed. Substantial epoxy absorption seems to have occurred if one assumes that aluminum undergoes minimal reflectance change under shock compression to 8 GPa (as is the case in Figures 4.13 and 4.14).

4.2.2 Chromium experiments

Two reverse chromium experiments—NSLS07-06 and NSLS07-19—were performed at 8 GPa. The results are shown in Figures 4.18 and 4.19. A minor impact flash was observed in both experiments. No changes are evident in the near visible spectrum, but minor reflectance increases were observed in the near-infrared and possibly the mid-infrared. The results of these two experiments appear to be highly consistent with one another.

4.2.3 Copper experiments

Two reverse copper experiments, NSLS07-17 and NSLS07-18, were performed at 8 GPa. The results are shown in Figures 4.20 and 4.21. No obvious reflectance changes were observed in experiment NSLS07-17. Near visible reflectance appears unchanged in experiment NSLS07-18, and there are minor reflectance increases in the near-infrared and first mid-infrared channels; the second mid-infrared channel has substantial baseline noise, complicating its interpretation.

4.2.4 Platinum experiments

Three reverse platinum experiments—NSLS07-07, NSLS07-20, and NSLS07-21—were performed at 8 GPa. The results are shown in Figures 4.22, 4.23, and 4.24. Apparent reflectance drops were observed in all three experiments, though NSLS07-20 seems anomalous in the amount of signal decrease and ultimate window failure. Reflectance change is

[1]The initial interpretation of this flash was that the AngstromBond become strongly emitted upon compressed to 8 GPa. However, these flashes are never observed in standard configuration experiments with an opaque sample (the chromium and high emissivity films were slightly transparent). Furthermore, similar flashes are observed in separate aluminum experiments using Loctite 326 epoxy (Section 4.3.1).

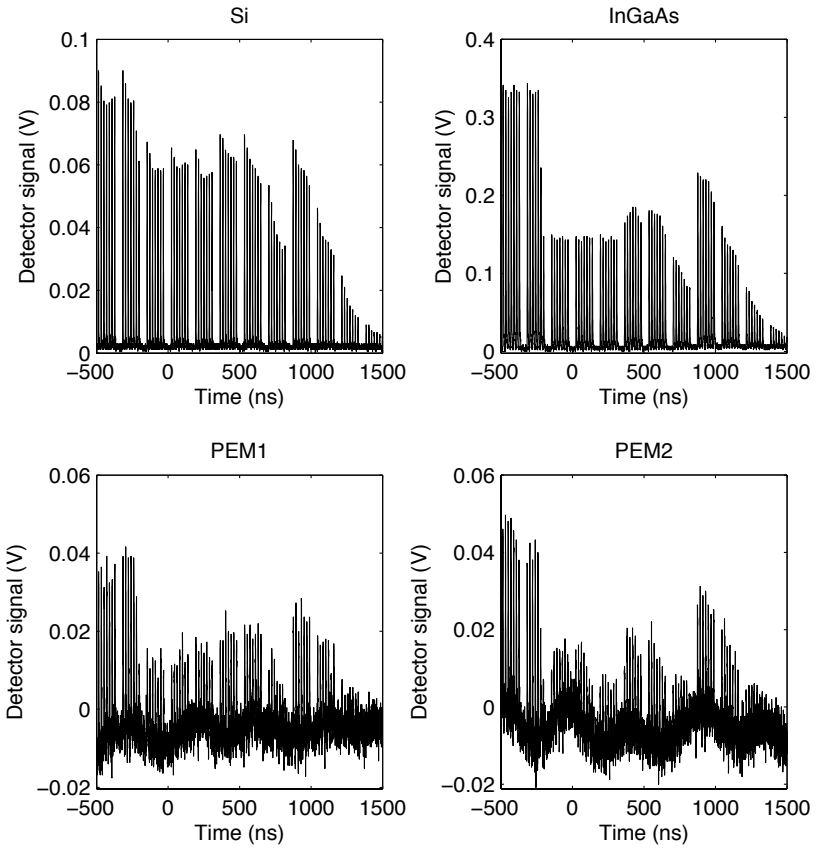

Figure 4.15. Raw signal data from NSLS07-13 (reverse Al at 8 GPa)

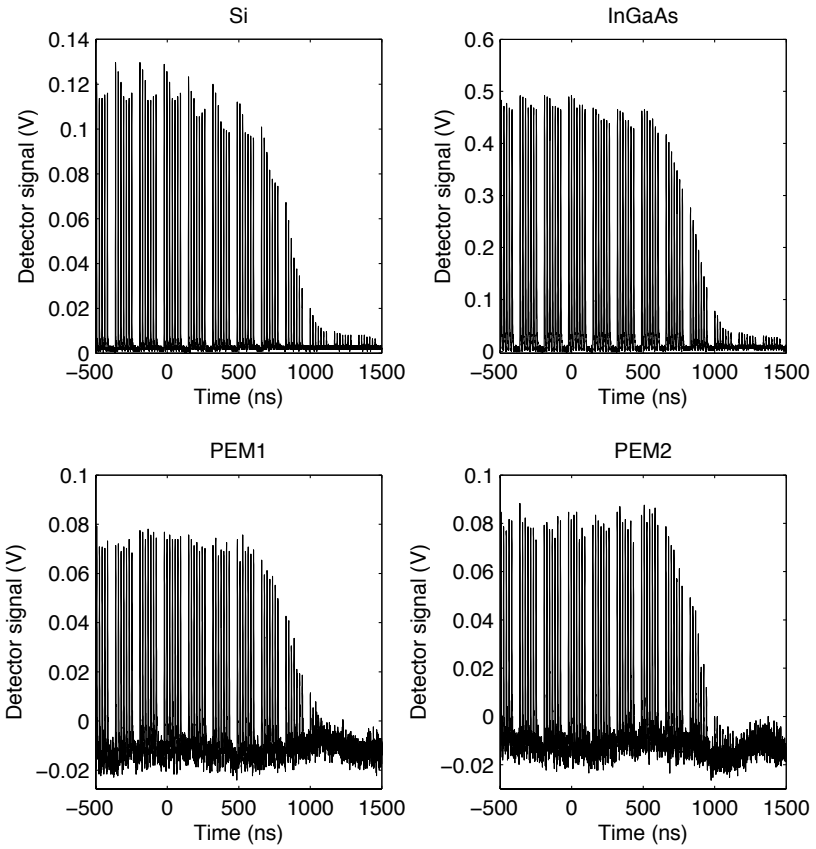

Figure 4.16. Raw signal data from NSLS07-14 (reverse Al at 8 GPa)

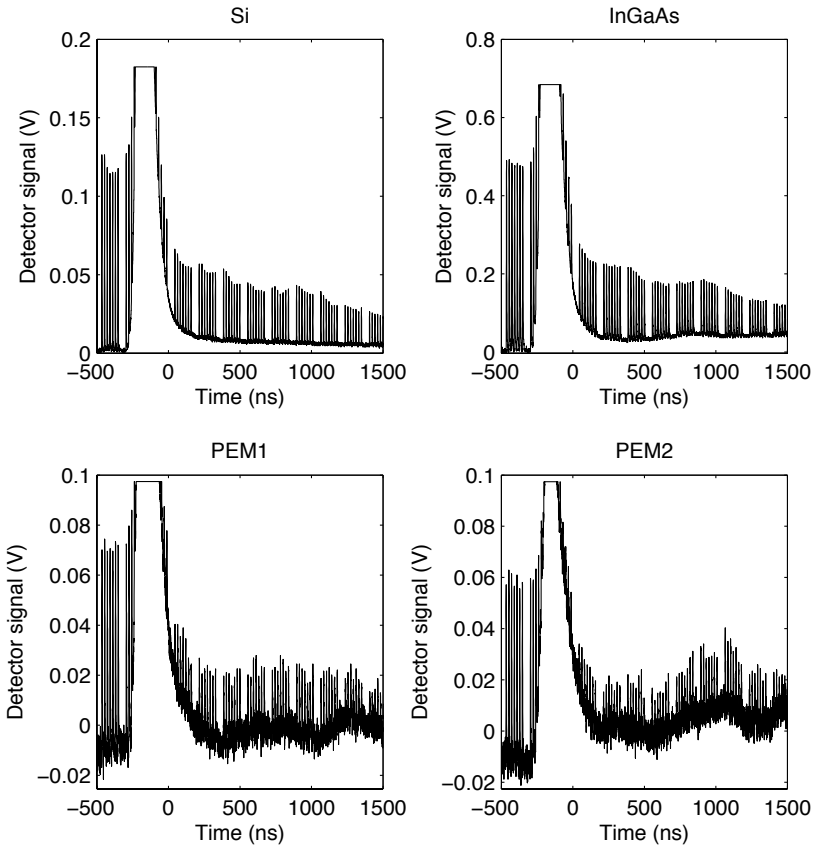

Figure 4.17. Raw signal data from NSLS07-15 (separate Al at 8 GPa)

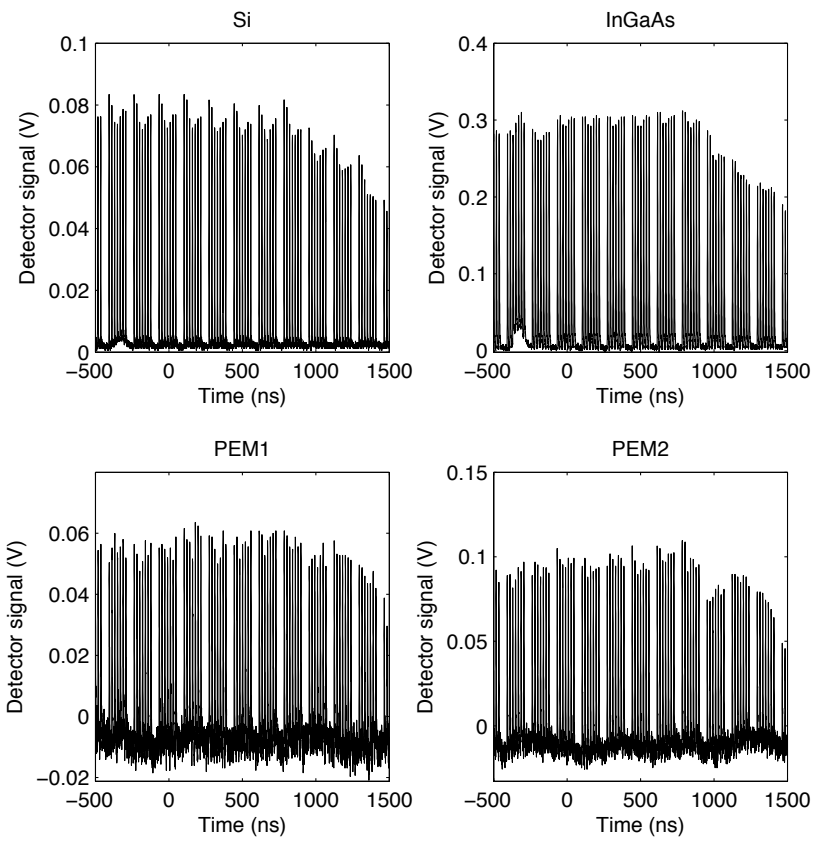

Figure 4.18. Raw signal data from NSLS07-06 (reverse Cr at 8 GPa)

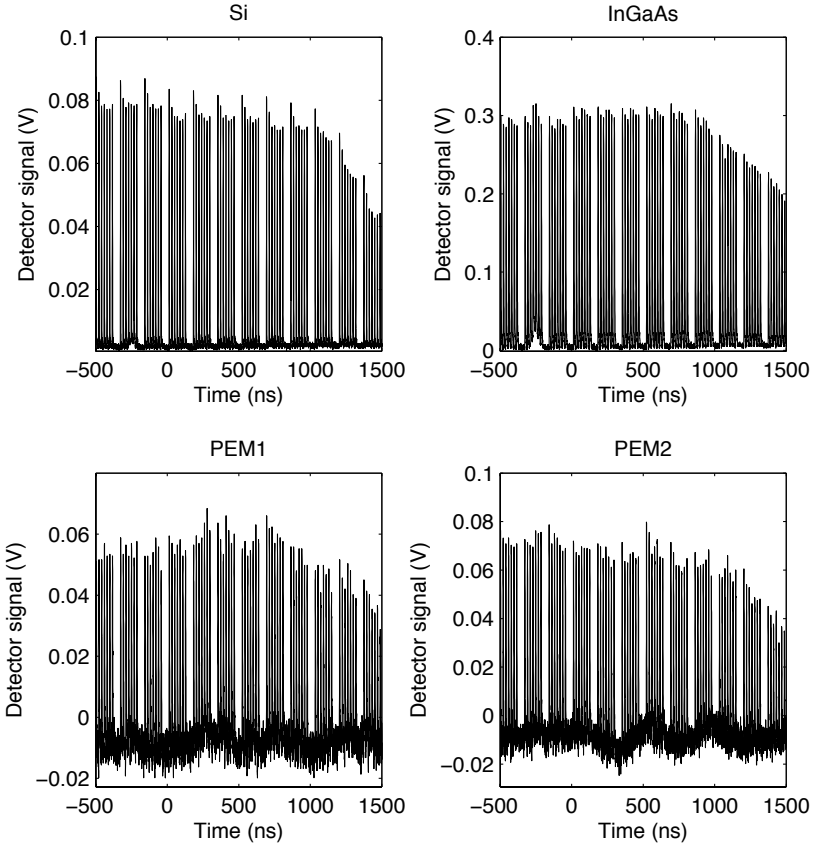

Figure 4.19. Raw signal data from NSLS07-19 (reverse Cr at 8 GPa)

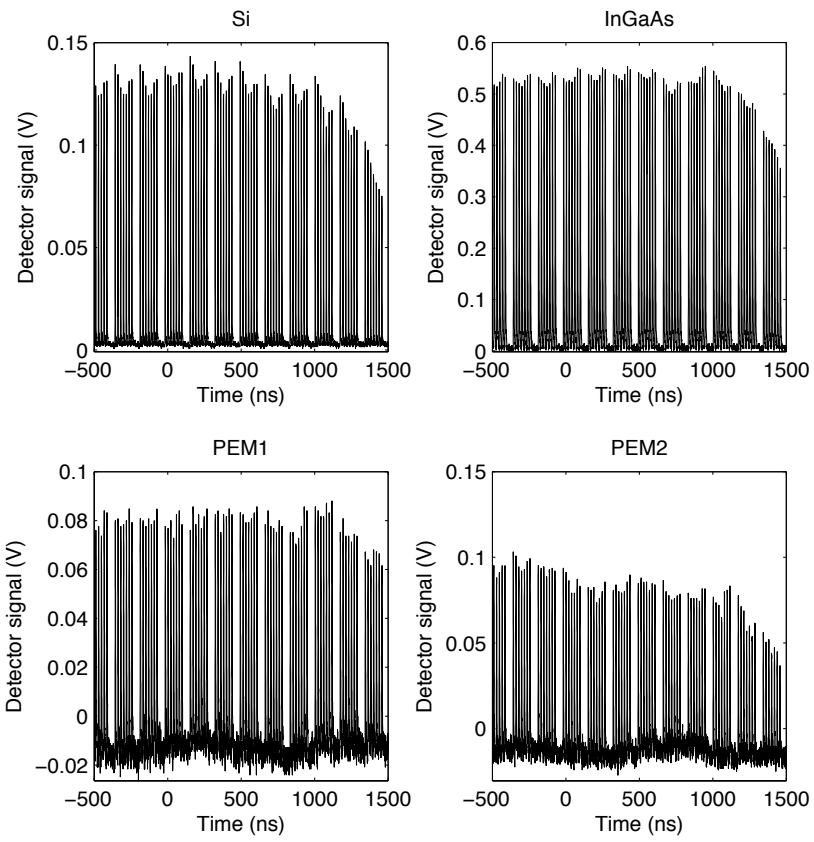

Figure 4.20. Raw signal data from NSLS07-17 (reverse Cu compressed to 8 GPa)

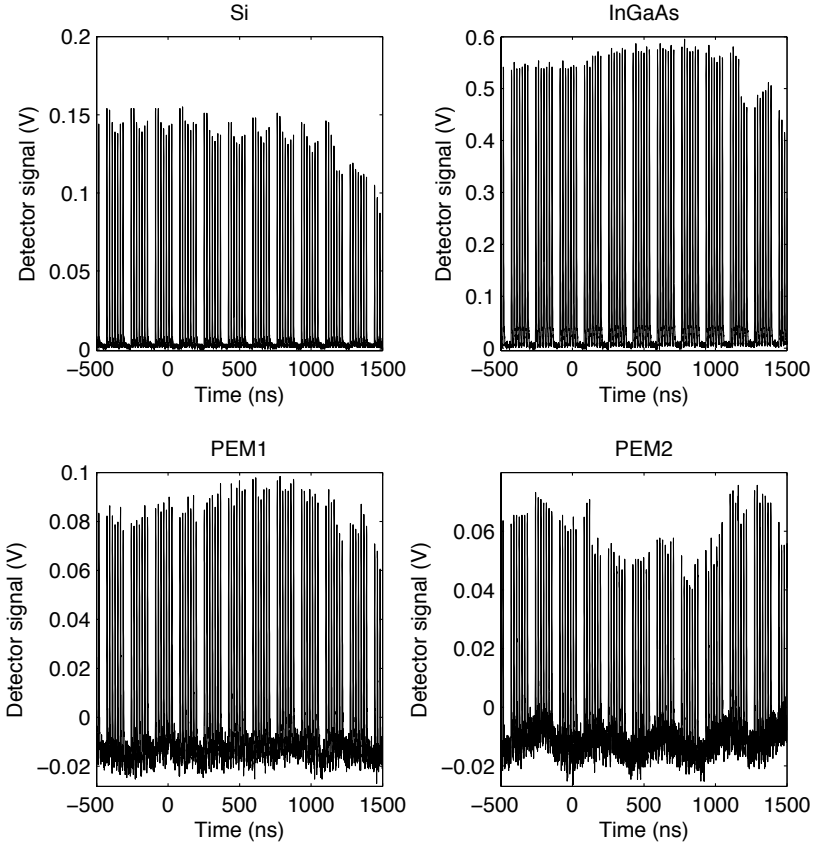

Figure 4.21. Raw signal data from NSLS07-18 (reverse Cu compressed to 8 GPa)

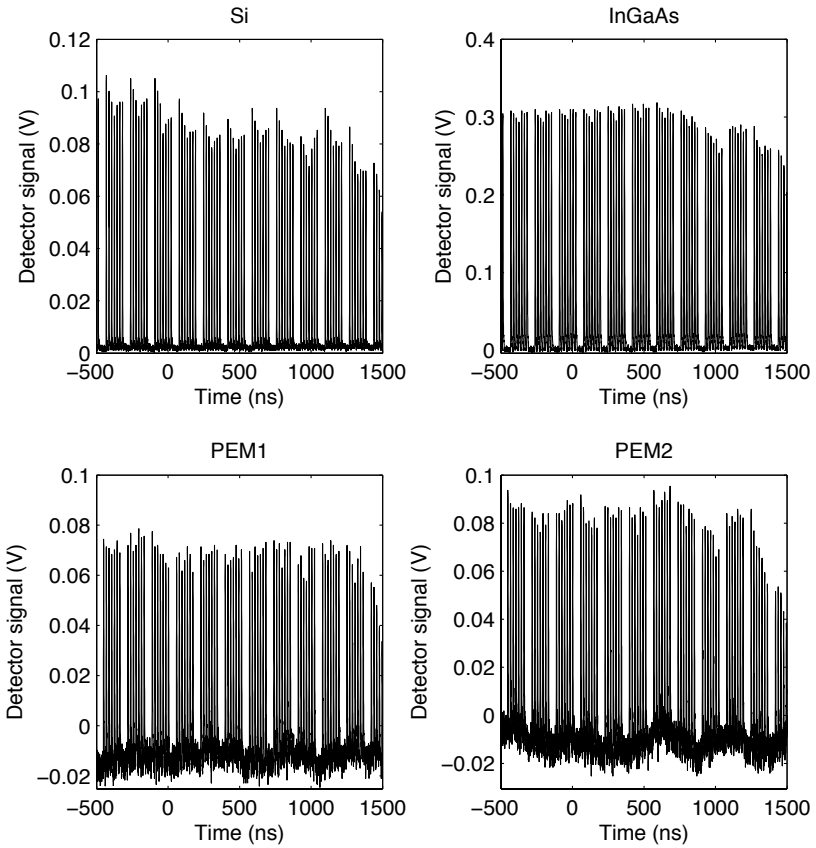

Figure 4.22. Raw signal data from NSLS07-07 (reverse Pt at 8 GPa)

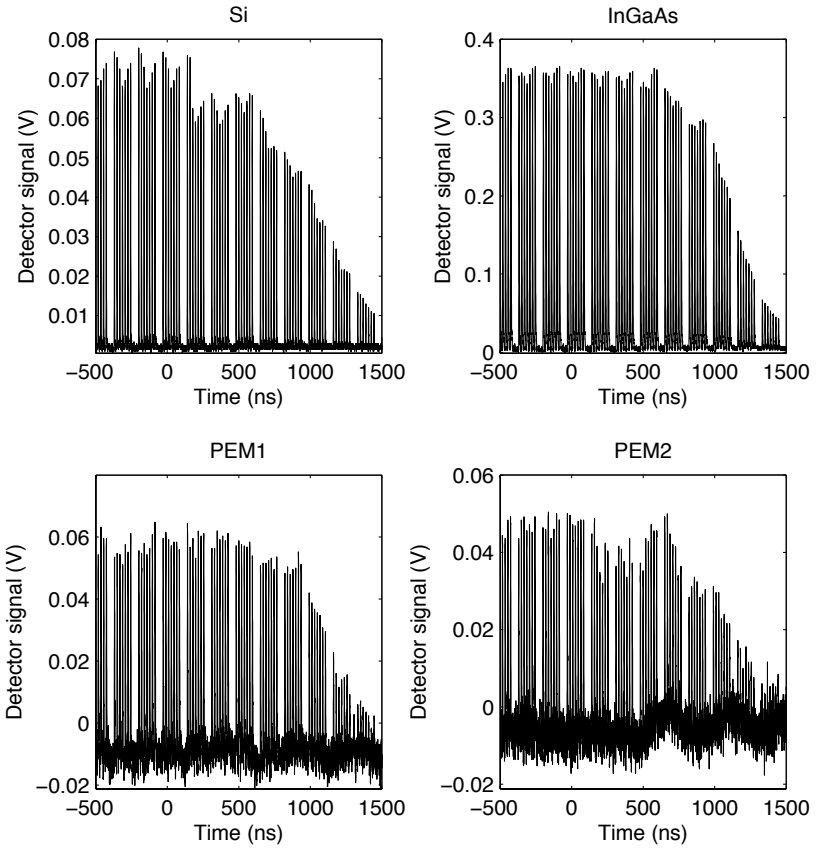

Figure 4.23. Raw signal data from NSLS07-20 (reverse Pt at 8 GPa)

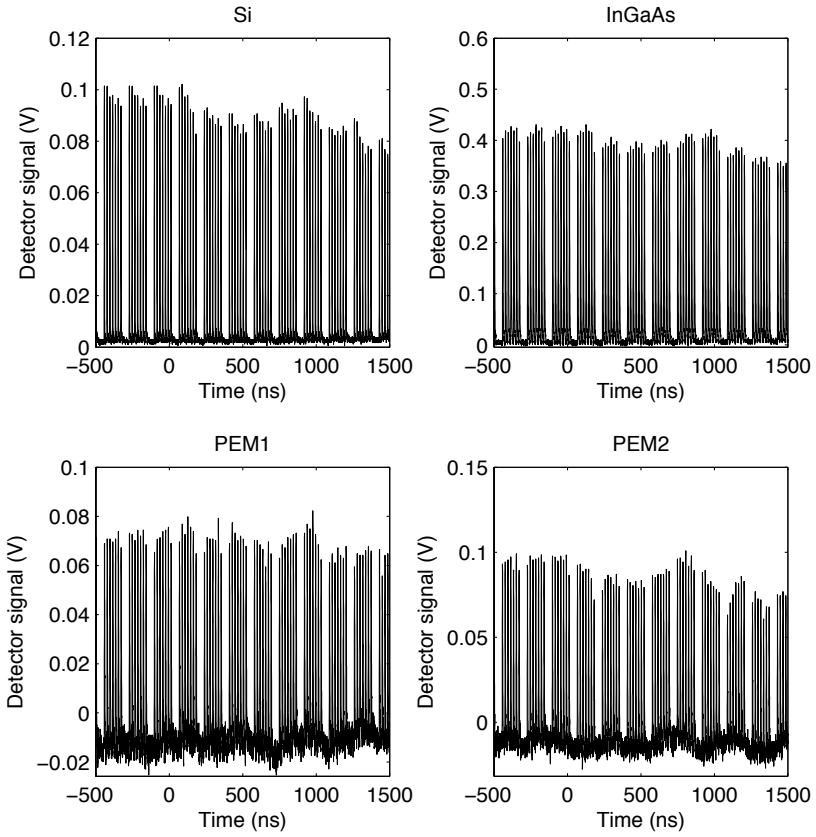

Figure 4.24. Raw signal data from NSLS07-21 (reverse Pt at 8 GPa)

most evident in the Si detector signal, and less obvious in the InGaAs signal. Reflectance decrease is somewhat apparent in the mid-infrared PEM signals, but the extent is obscured by base line drift.

4.2.5 High emissivity film experiments

Two standard high emissivity film experiments—NSLS07-09 and NSLS07-10—were performed near 5 GPa. The results are shown in Figure 4.25 and 4.26. Minor impact flashes were observed in both experiments, primarily on the Si and InGaAs channels with little obvious effect in the PEM channels. Apparent reflectance losses were observed in the Si and InGaAs channels in both experiments, though the magnitude of these losses does not appear to be consistent.

Two standard high emissivity experiments—NSLS07-05 and NSLS07-08—were performed at 8 GPa. The results of are shown in Figures 4.27 and 4.28. An impact flash across all four detectors occurred in both experiments. Similar apparent reflectance losses were observed on the first three channels in both experiments, but there is a discrepancy in the second PEM channel, where reflectance appears to decrease in NSLS07-05 and increase in NSLS07-08.

4.3 Campaign III (August 2007)

The third NSLS campaign took place August 23–31, 2007. The optical configuration from the second campaign was retained, with even greater emphasis on electromagnetic shielding (*e.g.*, conductive tape placed along all joints). To eliminate velocity variations from the experiment time line, an additional set of trigger pins was added to create pulses at the time of impact, rather than several microseconds before. The final timing configuration is shown in Figure 4.29.

Experiments performed during this campaign are summarized in Table 4.2. The focus of the campaign was to study different stack configurations of aluminum and the high emissivity film, the latter manufactured by both MPCL and organization 2452.

4.3.1 Aluminum experiments

Two separate aluminum experiments—NSLS07-32 and NSLS07-33—were performed at 8 GPa. The results are shown in Figures 4.30 and 4.31. As in the previous shot campaign, both experiments showed excessive impact flash, indicating that the flash is not likely to to emission from the bond layer.

Two reverse aluminum experiments—NSLS07-34 and NSLS07-35—were performed at 8 GPa. The results are shown in Figures 4.32 and 4.33. No change in apparent reflectance was observed in NSLS07-34, whereas systematic apparent reflectance losses were found in all NSLS07-35 measurements. A similar inconsistency was found in the previous shot campaign (Section 4.2.1), although substantially better signal quality was obtained in the

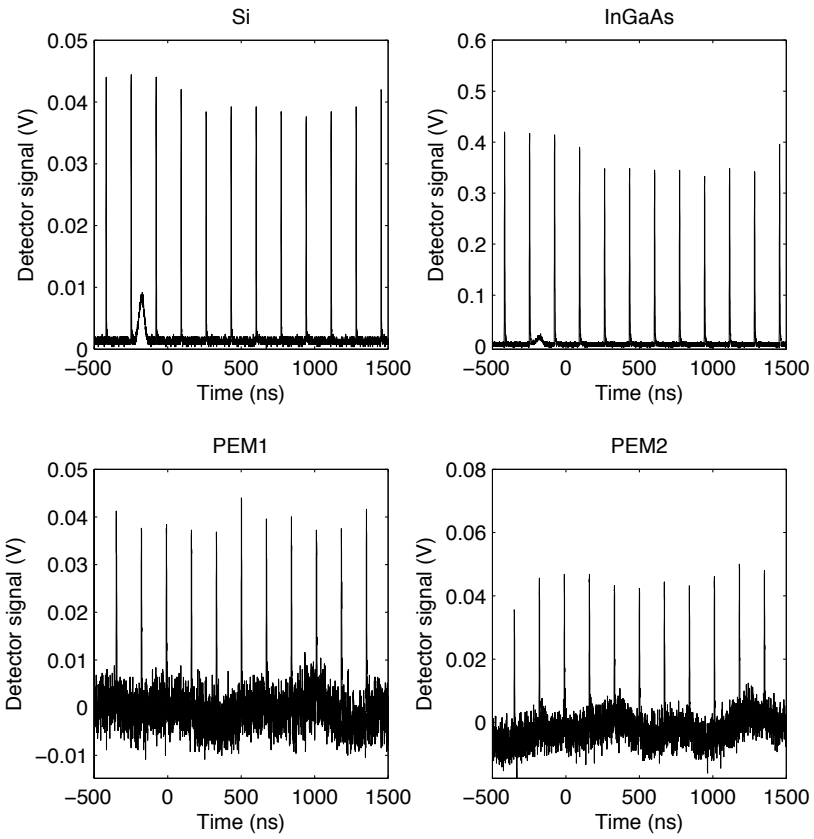

Figure 4.25. Raw signal data from NSLS07-09 (standard high ε film at 5 GPa)

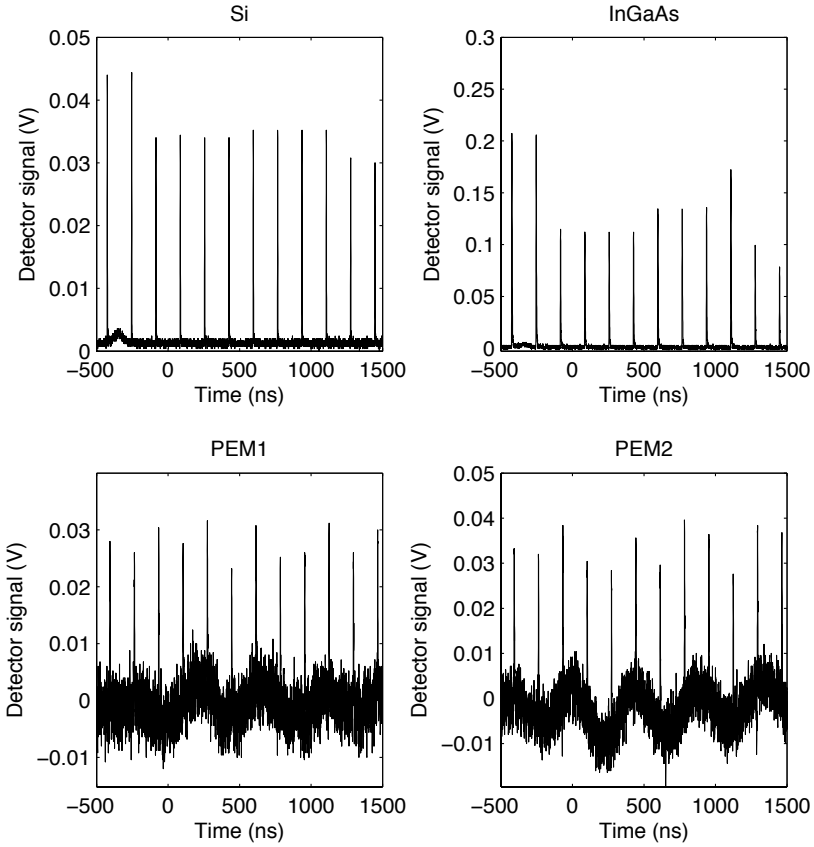

Figure 4.26. Raw signal data from NSLS07-10 (standard high ε film at 5 GPa)

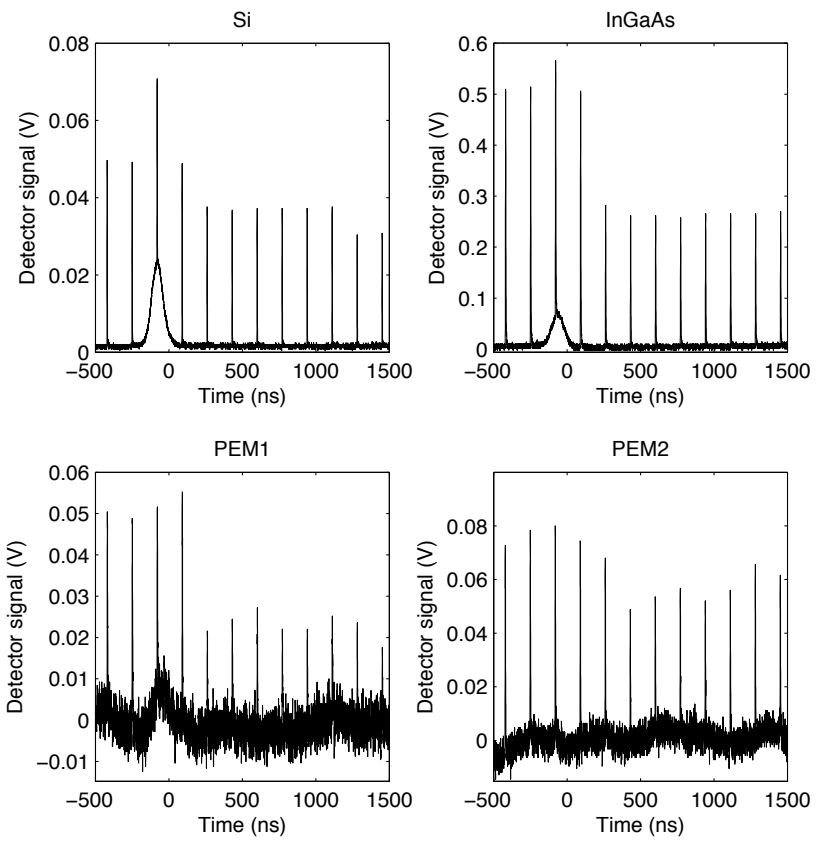

Figure 4.27. Raw signal data from NSLS07-05 (standard high ε film at 8 GPa)

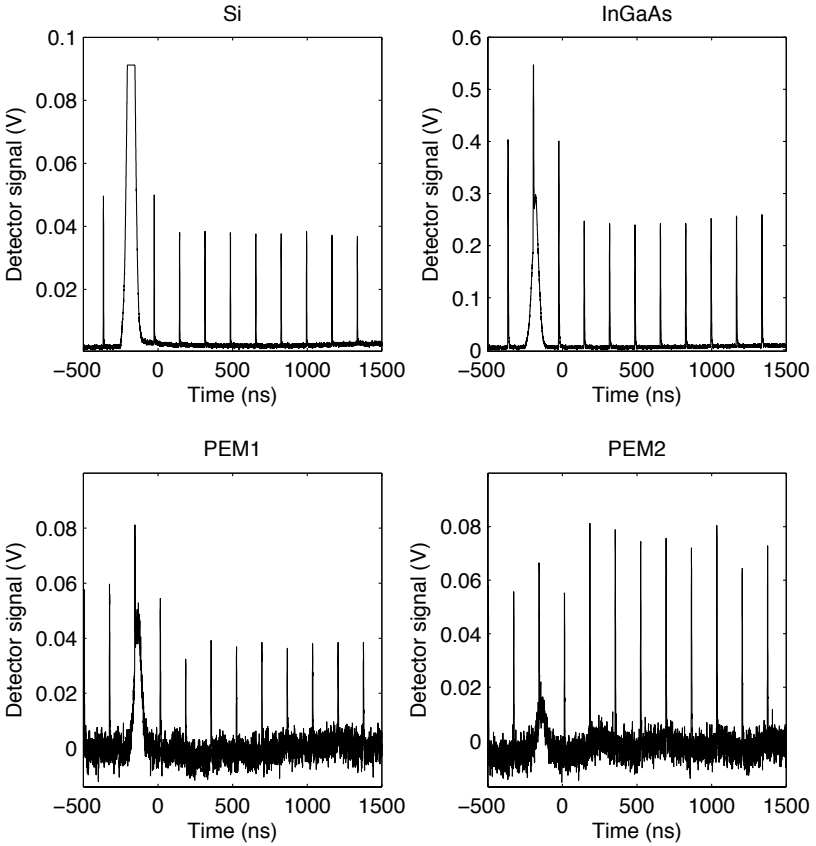

Figure 4.28. Raw signal data from NSLS07-08 (standard high ε film at 8 GPa)

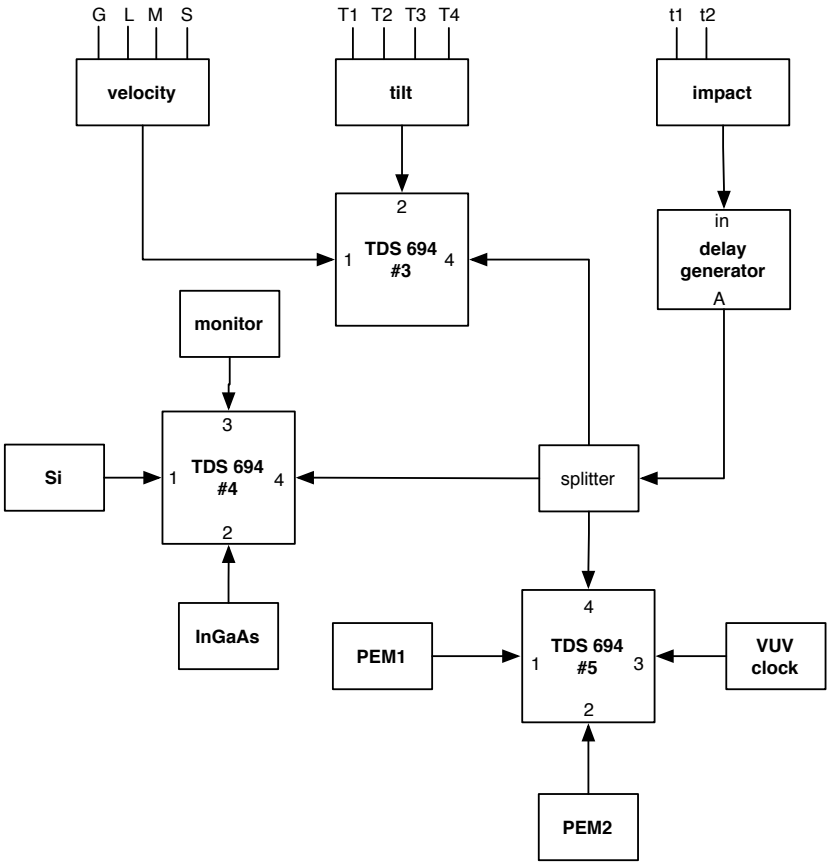

Figure 4.29. Timing setup for August 2007 experiments

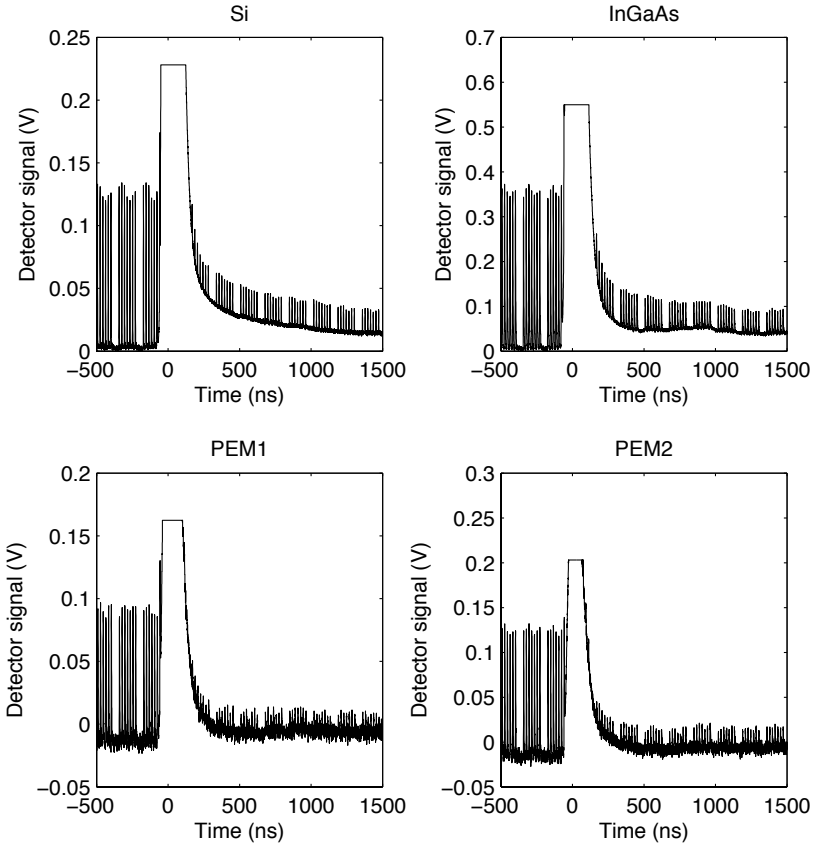

Figure 4.30. Raw signal data from NSLS07-32 (separate Al at 8 GPa)

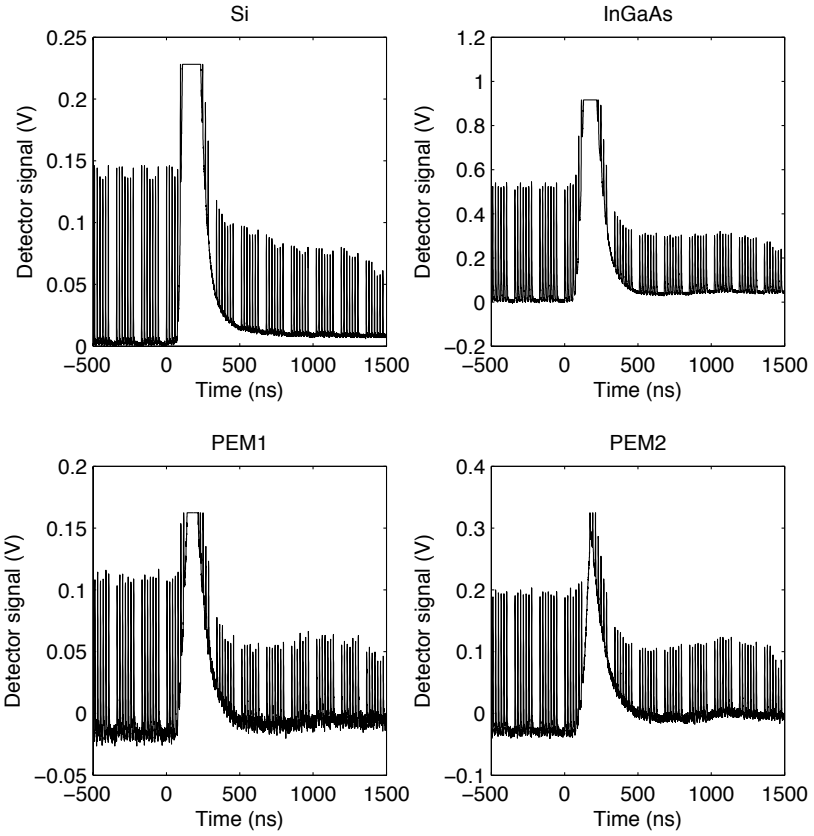

Figure 4.31. Raw signal data from NSLS07-33 (separate Al at 8 GPa)

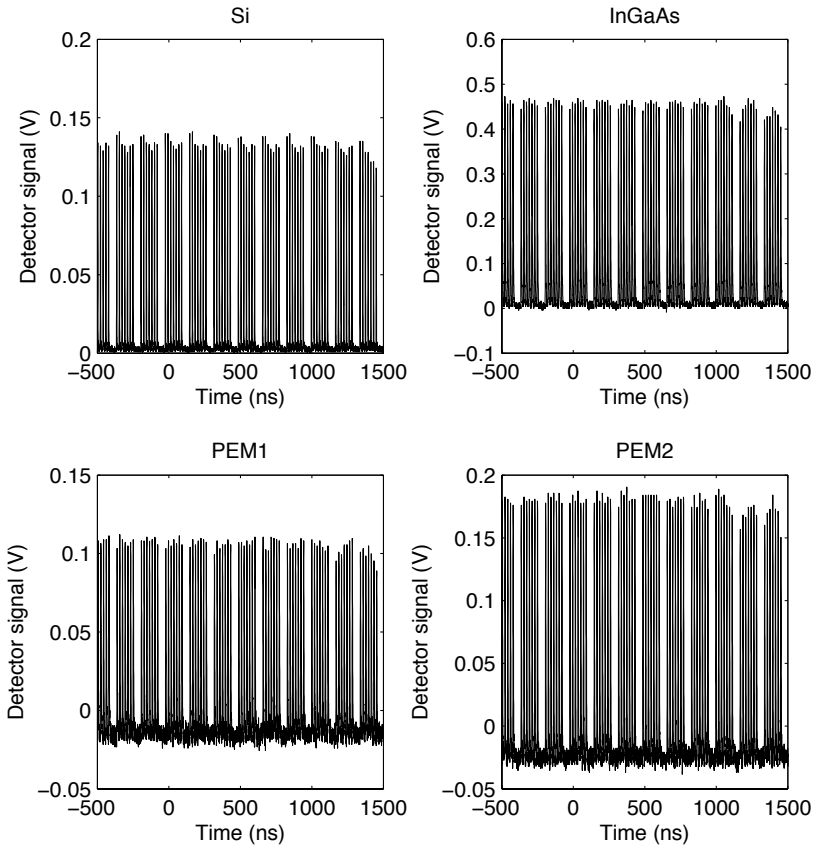

Figure 4.32. Raw signal data from NSLS07-34 (reverse Al at 8 GPa)

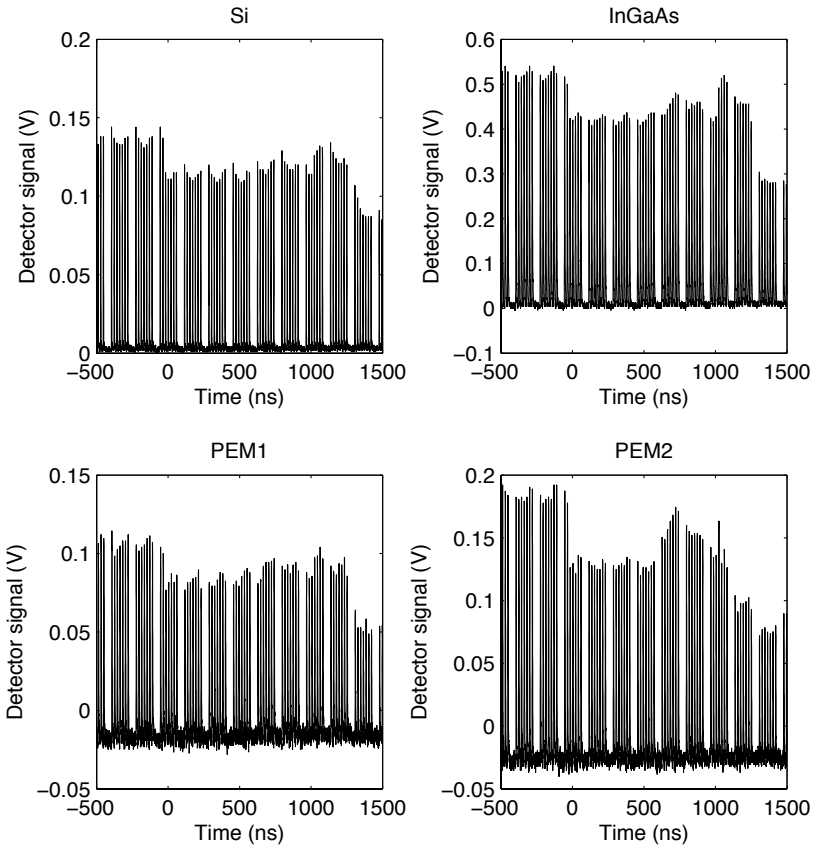

Figure 4.33. Raw signal data from NSLS07-35 (reverse Al at 8 GPa)

Table 4.3. NSLS campaign III summary. Samples fabricated by MPCL and organization 2452 as noted.

ID	configuration	sample	bond	v_{imp} (m/s)
NSLS07-32	separate	Al†	Loctite 326	385
NSLS07-33	separate	Al†	Loctite 326	348
NSLS07-34	reverse	Al†	Loctite 326	383
NSLS07-35	reverse	Al†	Loctite 326	373
NSLS07-24	reverse	high $\varepsilon^{\dagger}$	Loctite 326	382
NSLS07-25	reverse	high $\varepsilon^{\dagger}$	Loctite 326	381
NSLS07-26	reverse	high ε^{*}	Loctite 326	378
NSLS07-27	reverse	high ε^{*}	Loctite 326	380
NSLS07-28	standard	high ε^{*}	Loctite 326	375
NSLS07-29	standard	high ε^{*}	Loctite 326	382
NSLS07-31	standard	high $\varepsilon^{\dagger}$	Loctite 326	371

* MPCL coating
† org. 2452 coating

third campaign.

4.3.2 High emissivity film experiments

Four reverse high emissivity sample experiments—NSLS07-24, NSLS07-25, NSLS07-26 and NSLS07-27—were performed at 8 GPa. The first two experiments involved samples fabricated by organization 2452, while the second two experiments were prepared by MPCL. The results of these experiments are shown in Figures 4.34–4.36. Impact flash was observed in all four experiments. In the first two experiments, a consistent loss of apparent reflection was observed across all detectors. The second two experiments are not nearly so consistent, with decreasing reflectance in NSLS07-26 and increasing reflectance in NSLS07-27.

Three standard high emissivity sample experiments—NSLS07-28, NSLS07-29, and NSLS07-31—were performed at 8 GPa. Samples in the first two experiments were fabricated at MPCL, while the third experiment sample was created by organization 2452. The results of these experiments are shown in Figures 4.38–4.40. As in the reverse experiments described above, impact flash was observed in all three experiments. Similar trends were observed in the first two experiments, where apparent reflectance remained fixed or decreased; the magnitude of these decreases varied slightly between experiments (particularly for the InGaAs channel). The third experiment also showed similar trends, although the reflectance decrease is more pronounced.

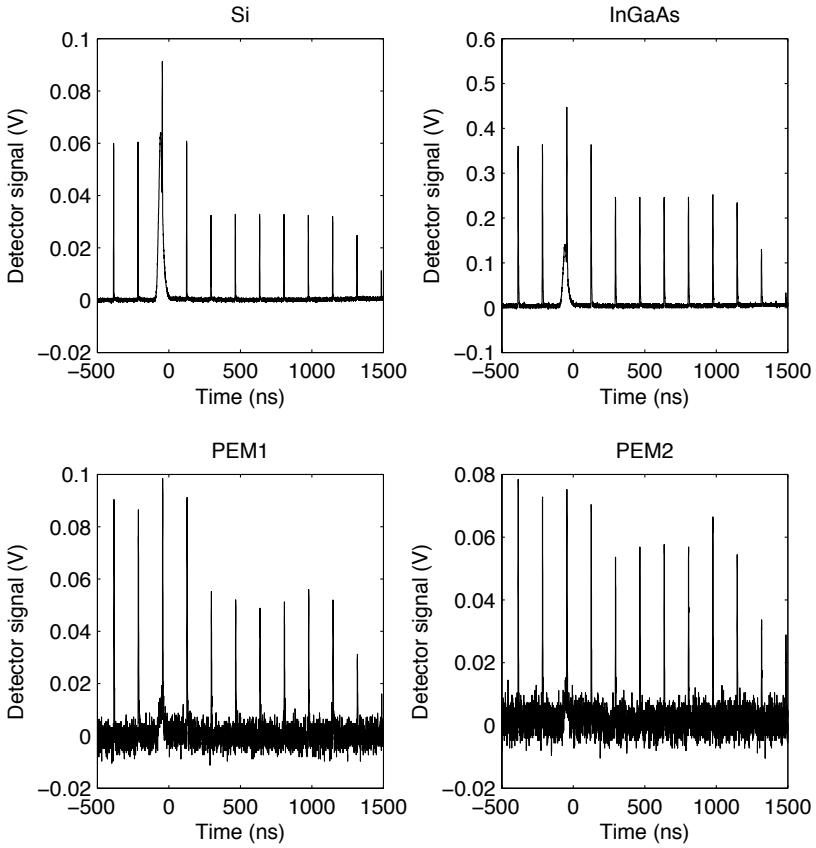

Figure 4.34. Raw signal data from NSLS07-24 (reverse high emissivity film at 8 GPa). The coating was manufactured by organization 2452.

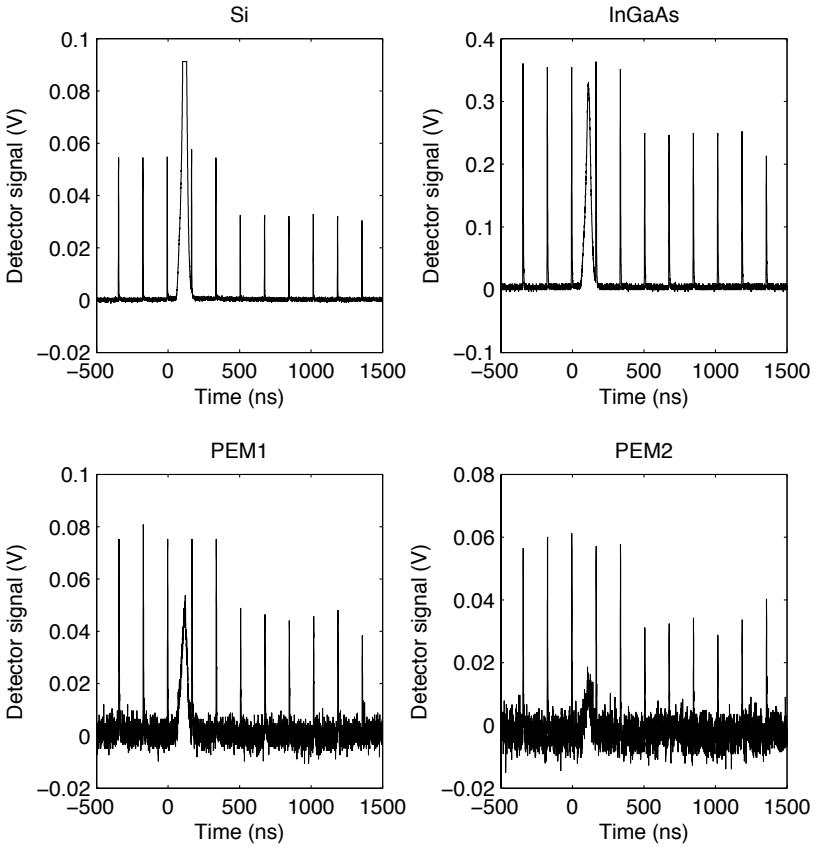

Figure 4.35. Raw signal data from NSLS07-25 (reverse high emissivity film at 8 GPa). The coating was manufactured by organization 2452.

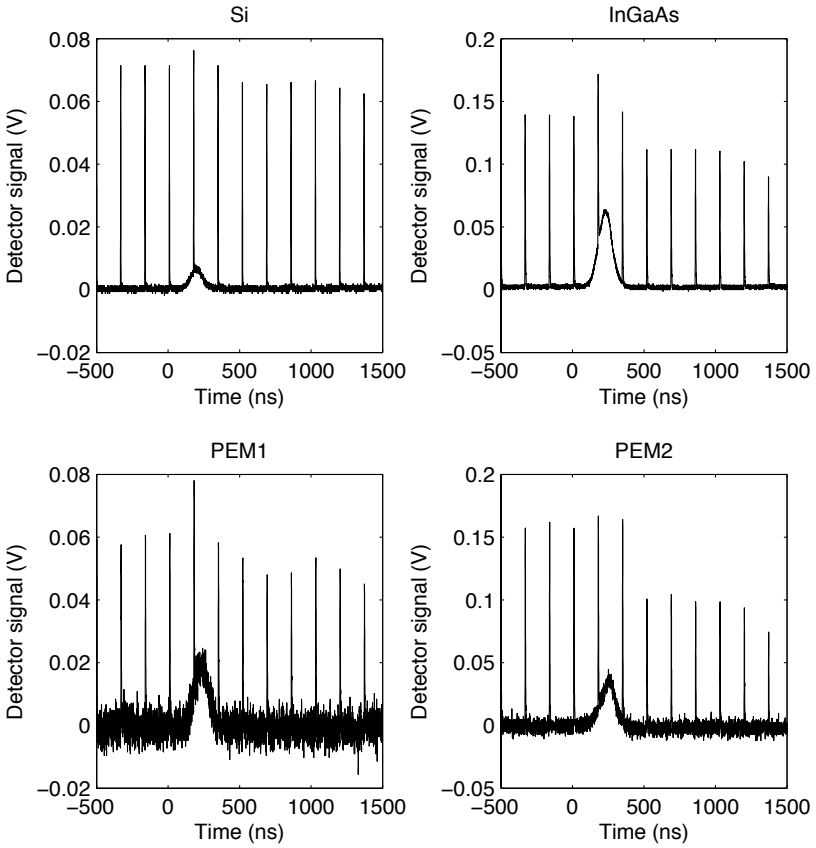

Figure 4.36. Raw signal data from NSLS07-26 (reverse high emissivity film at 8 GPa). The coating was manufactured by organization MPCL.

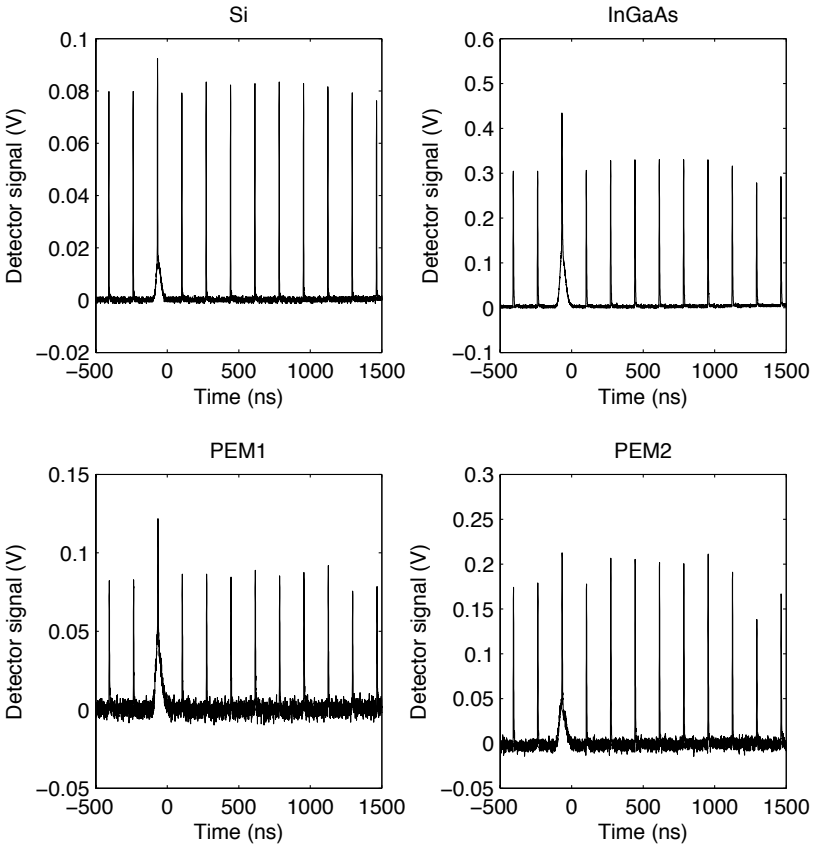

Figure 4.37. Raw signal data from NSLS07-27 (reverse high emissivity film at 8 GPa). The coating was manufactured by organization MPCL.

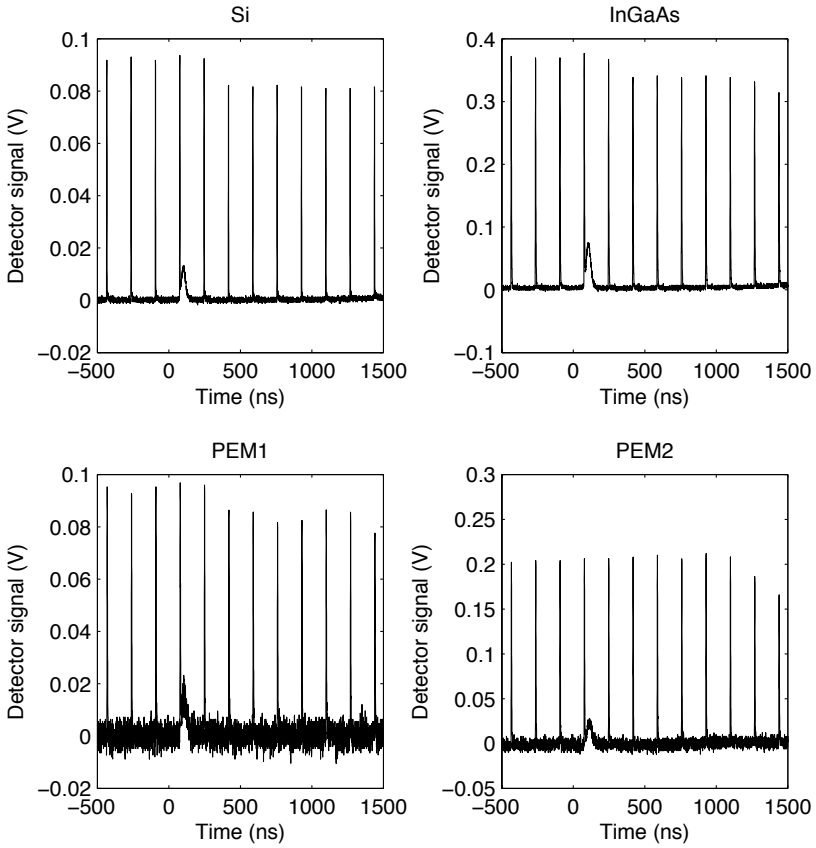

Figure 4.38. Raw signal data from NSLS07-28 (standard high emissivity film at 8 GPa)

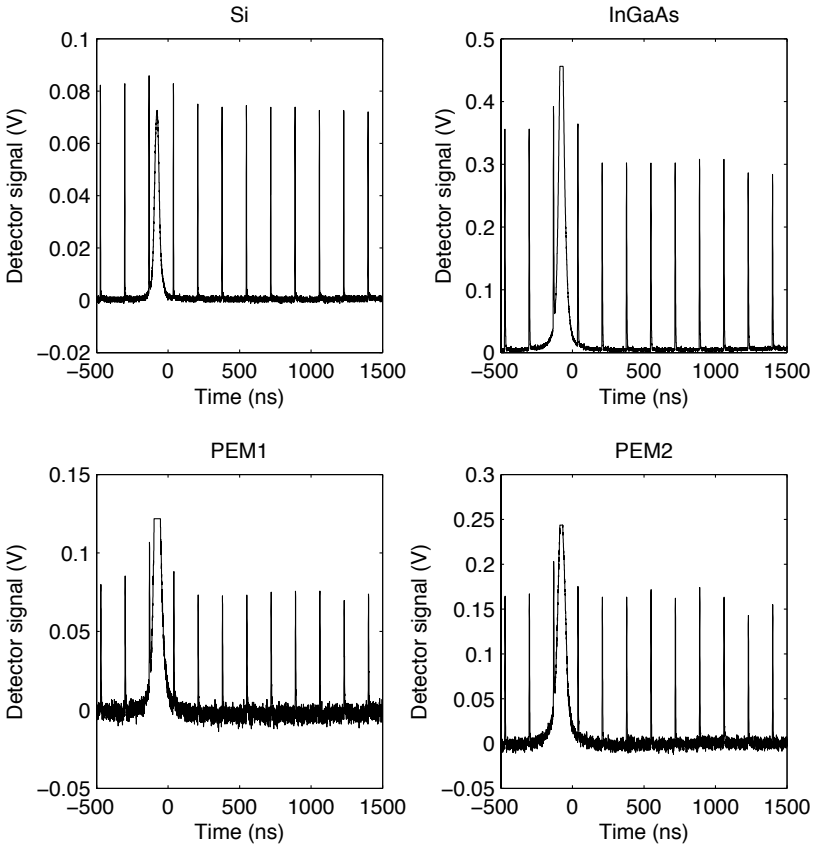

Figure 4.39. Raw signal data from NSLS07-29 (standard high emissivity film at 8 GPa)

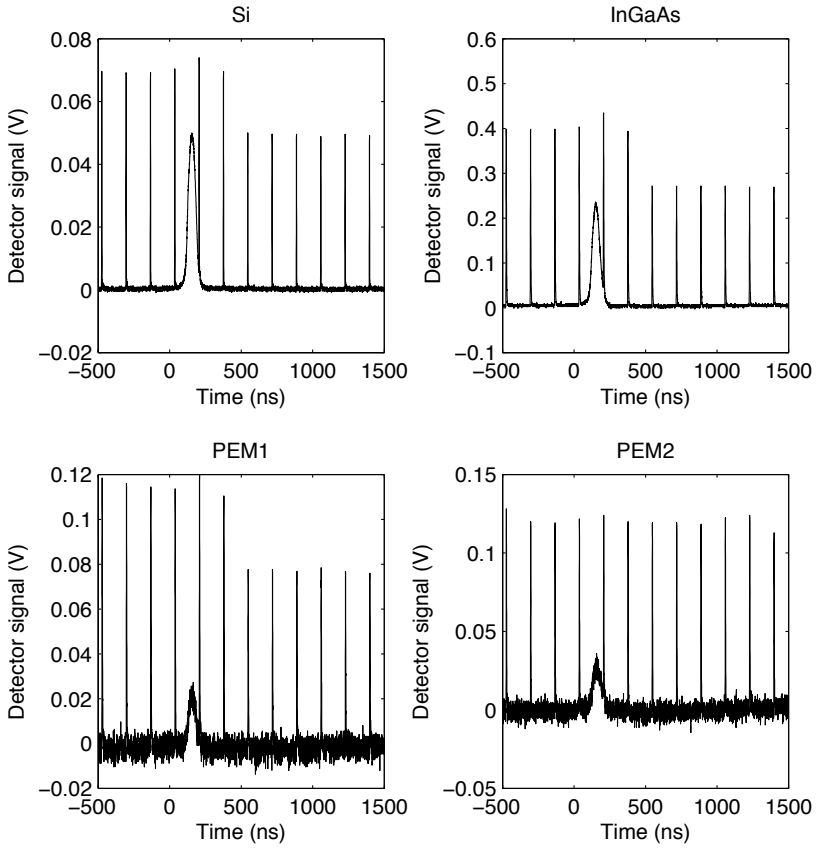

Figure 4.40. Raw signal data from NSLS07-31 (standard high emissivity film at 8 GPa)

CHAPTER 5

Analysis and discussion

This chapter presents analysis and discussion of the results from the previous chapter. Experimental results are treated in the first three sections based on target configuration—reverse, standard, and separate. This division is useful because each configuration has similar characteristics and limitations. The next section presents an preliminary interpretation of the results. The final section describes a method of reducing the measured data signals into a more useful form, which may help reduce non-ideal aspects of dynamic reflectance measurements.

5.1 Reverse sample configuration

The reverse configuration provides the most straightforward reflectance measurement in this work. Table 5.1 summarizes the reverse configuration experiments performed in this project. The peak stress in all experiments was approximately 8 GPa. Five sample materials—aluminum, chromium, copper, platinum, and the high emissivity coating—were studied in this configuration. Different behavior and trends were found among experiments involving a particular material.

First, consider the aluminum experiments (NSLS07-13, NSLS07-14, NSLS04-34, and NSLS07-35), where from previous VISAR experiments [15] one would expect little or no reflectance change. In two of these experiments, sample reflectance appears to remain unchanged by the compression to 8 GPa, whereas the remaining two experiments show consistent loss across the measured spectrum. All four experiments were fabricated by sputtering (organization 2452), but otherwise there is no common trait that would explain this discrepancy. The observation of reflectance decrease occurred between two different campaigns (II and III) and bonding materials (AngstromBond and Loctite 326), eliminating these factors from consideration.

Unlike the aluminum experiments, reverse chromium measurements (NSLS07-06 and NSLS07-19) were nearly identical to one another across all measured spectral bands. Minor near-infrared reflectance increases were detected in both experiments, but otherwise no substantial reflectance changes were observed.

Table 5.1. Summary of reverse reflectance experiments. The peak stress in all experiments was 8 GPa.

Experiment	Sample	Reflectance changes
NSLS07-13	Al	Consistent loss
NSLS07-14	Al	No change
NSLS07-34	Al	No change
NSLS07-35	Al	Consistent loss
NSLS07-06	Cr	Minor near-IR increase
NSLS07-19	Cr	Minor near-IR increase
NSLS07-17	Cu	No change
NSLS07-18	Cu	Minor near-IR increase
NSLS07-07	Pt	Moderate near-visible and mid-IR decrease
NSLS07-20	Pt	Moderate near-visible and mid-IR decrease
NSLS07-21	Pt	Moderate near-visible, near-IR, and mid-IR decrease
NSLS07-24	High ε	Consistent loss
NSLS07-25	High ε	Consistent loss
NSLS07-26	High ε	Consistent loss
NSLS07-27	High ε	Slight increase

Reverse copper experiments (NSLS07-14 and NSLS07-18) showed similar behavior to the chromium samples: no reflectance changes on most channels. Unlike the chromium measurements, there is a discrepancy in the near-infrared region, where one experiment shows no change while another showed a minor reflectance increase.

In all platinum experiments (NSLS07-07, NSLS07-20, and NSLS07-21), there was a clear decrease in apparent reflectance in the near-visible and mid-infrared channels. The last experiment (NSLS07-21) also shows a a minor decrease in near-infrared reflectance, which is not observed in the other two experiments.

Three high emissivity film experiments (NSLS07-24, NSLS07-25, and NSLS07-26) showed considerable loss in apparent reflectance across all detector channels. Sample in the first two experiments were obtained from the same source (organization 2452), and show fairly similar reflectance loss on all but the farthest mid-infrared channels; the third experiment showed less reflectance loss, but was manufactured in a slightly different fashion (MPCL). The fourth high emissivity film experiment (NSLS07-27) was distinct from the first three, indicating a slight increase in sample reflectance on compression.

Table 5.2. Summary of standard reflectance experiments. Except where noted, the peak stress in all experiments was 8 GPa.

Experiment	Sample	Reflectance changes
NSLS06-14	Al	No change
NSLS06-21	Al	Consistent loss
NSLS07-11	Al	Strong near-visible loss, minor IR losses
NSLS07-12	Al	Strong near-visible loss, minor IR losses
NSLS06-18	Cr	Near-infrared loss
NSLS06-20	Cr	Near-infared loss
NSLS06-19	Cu	Consistent loss
NSLS06-17*	high ε	Near-infrared loss
NSLS07-09*	high ε	Minor near-visible, near-IR losses
NSLS07-10*	high ε	Minor near-visible, near-IR losses
NSLS06-15	high ε	Near-infrared loss, mixed IR behavior
NSLS06-22	high ε	Near-infrared loss, mixed IR behavior
NSLS07-05	high ε	Strong near-visible and IR losses
NSLS07-08	high ε	Strong near-visible and IR losses
NSLS07-28	high ε	Minor loss on all but PEM2
NSLS07-29	high ε	Minor loss on all but PEM2
NSLS07-31	high ε	Consistent loss

*5 GPa peak stress

5.2 Standard sample configuration

The standard target configuration is complicated by the fact that light must pass through the bonding layer. Hence, the apparent reflectance measurement can be altered by both changes in actual sample reflectance and the transparency loss in the bond layer. Table 5.2 summarizes the standard configuration experiments performed in this project. Experiments were performed at peak pressures of 5 and 8 GPa as noted.

Four standard aluminum experiments (NSLS06-14, NSLS06-21, NSLS07-11, and NSLS07-12) were performed in the standard configuration. The first experiment showed no change in apparent reflectance, while reflectance loss was observed across all detector channels in the second experiment. Strong near-visible losses were observed in the third and fourth experiments, with minor losses across the infrared channels. The latter experiments differed in their use of bonding material (AngstromBond in NSLS07-11, Loctite 326 in NSLS07-12), ruling out material specific absorption as source of apparent reflection loss.

Near-infrared reflectance losses were observed in both standard chromium experiments (NSLS06-18 and NSLS06-20). Results in the mid-infared are mixed: one experiment (NSLS06-18) shows a minor increase on one channel and a decrease on another, while

the other experiment (NSLS06-20) shows moderate and minor reflectance increases on the same channels.

One standard configuration copper experiment (NSLS06-19) was performed. Reflectance loss was observed on all detector channels.

Three 5 GPa experiments were performed on the standard configuration high emissivity films. The first experiment (NSLS06-17) used an MPCL sample, and showed significant reflectance loss in the mid-infrared with a possible mid-infrared reflectance increase (one channel was lost during the shot). Minor near-visible and near-infrared reflectance losses were also observed in experiments NSLS07-09 and NSLS07-10 (organization 2452 material), and near-infared changes seem minimal.

Seven 8 GPa experiments were performed on the standard configuration high emissivity films. Similar to the first 5 GPa result, experiments NSLS06-15 and NSLS06-22 (MPCL material) indicate strong reflectance decrease in the near-infrared; mid-infrared results were mixed between increasing and decreasing reflectance. Repeatable near-visible and infrared (other than the longest channel) losses were observed in experiments NSLS07-05 and NSLS07-08, which utilized samples from organization 2452; both reflectance increase and decrease was observed on the longest mid-infrared channel. Minor losses across all channels (except the longest infrared channel) were also observed in experiments NSLS07-28 and NSLS07-29 using MPCL coatings; similar trends (of larger magnitude) were also observed for the organization 2452 coating in experiment NSLS07-31.

5.3 Separate sample configuration

Three separate configuration aluminum experiments were performed in this project, and the results are summarized in Table 5.3. Each experiment was performed at a peak pressure of 8 GPa.

One separate target (NSLS07-15) was held together with AngstromBond while the remaining targets (NSLS07-32 and NSLS07-33) used Loctite 326. The experiment results were very similar with one another, and strikingly different from the other configurations. A substantial impact flash, often resulting in digitizer saturation, was observed in all three experiments. In addition to being much brighter than impact flashes in the standard and reverse configurations, emission in the separate configuration is much longer lived, lasting several hundred nanoseconds followed by a low level emission over longer time scales. A clear decrease in reflected signal occurs after impact, but the long emission duration makes it impossible to determine if the transition occurs during impact or compression of the bond layer several hundred nanoseconds later.

Initially, the bright flash observed in separate configuration experiments was attributed to emission by AngstromBond epoxy during its initial compression. Subsequent observations of a similar flash with Loctite 326, which is known not to flash when compressed to even higher stresses [6], brought this interpretation into question. If one assumes that the flash

Table 5.3. Summary of separate reflectance experiments.

Experiment	Sample	Reflectance changes
NSLS07-15	Al	Loss on all channels
NSLS07-32	Al	Loss on all channels
NSLS07-33	Al	Loss on all channels

is due interface closure at impact, the natural question is why this flash is so much brighter than in other configuration? There are two possible explanations that may simultaneously play a role. First, the optical relay in a separate configuration experiment is focused at the impact surface, so light generated there is more efficiently coupled to the detectors than it would be in a standard or reverse configuration experiment (where the optics are focused roughly 1.6 mm behind the impact surface). Second, the deposited aluminum sample in a separate configuration experiment is exposed throughout the assembly, shipping, and alignment process, which may allow pinholes to form. By comparison, samples in standard and reverse configuration experiments are only exposed to air between the short time between deposition and stack assembly (typically, a few days), and no direct handling of the coating is needed. Thus, impact flash may pass through sample pinholes in separate configuration experiment, whereas even slightly transparent standard and reverse configuration experiments are uniformly opaque.

5.4 Interpretation

Due to several technical challenges, it is difficult to make quantitative assessments in this work. After reviewing these challenges, several qualitative conclusions can be made.

5.4.1 Challenges

Interpreting apparent reflectance changes is difficult for several reasons. Conceptually, the sample is viewed as an isolated free surface, but reflection takes place at an interface beneath one or more material layers. This interface is non-stationary, and may become tilted from its original configuration (from which the optical relay is optimized). The challenges in properly interpreting apparent reflectance measurements fall into three general categories: geometric, spectroscopic, and diagnostic.

Sample changes that alter the geometry of light reflection, rather than actual absorption, are a potentially important to the interpretation of this work. Examples of geometric change are target motion, impact tilt, and specular-diffuse transformations. Given the long focal length mirrors used to direct light to and collect light from the target, target motion does

not play a substantial role in this work.[1] Impact tilt could be an issue—the impact tilt of the 3" gun in this project is on the order of 2 milliradians, which under symmetric impact would tilt the sample by about 1 milliradian [16]. Diffuse reflection in the sample or diffuse transmission in the bond layer (standard and separate configurations only) might also divert light outside the optical relay's collection angle, showing up as a loss in apparent reflection. One would expect tilt-induced losses to be largely independent of wavelength, and diffuse effects should monotonically decrease with increasing wavelength.

Spectroscopic changes in the target system, particularly the bond layer, are another area of concern. Throughout this work, it is assumed that the transparency of sapphire remains unchanged throughout the compression experiment. Infrared absorption of the epoxy is thought to be minimal, particularly for Loctite 326. Interference effects, however, are an open question. White light fringes were clearly visible in most of the target stacks, indicating bond thicknesses on the order of a few optical wavelengths. As the bond is compressed by the shock wave, the interference pattern may change. The role of such interference on interpretation of dynamic reflectance (or emission, for that matter) has not been thoroughly addressed at this time.

Finally, interpretation of this work is complicated by several diagnostic limitations. The coarse spectral resolution (four channels spanning 800–4500 nm) obscures all but the most broad reflectance changes. As such, one cannot readily discern overall reflectance increase from a spectral shift within a several hundred nanometer range. Further problems are encountered in the mid-infrared, where the high speed PEM detectors used to resolve individual synchrotron pulses are prone to substantial noise and baseline variations. Some improvements were made during this project, primarily by increased electromagnetic shielding, but the performance of these channels is no where near that of the InGaAs and Si channels.

5.4.2 Metal reflectance

Despite the technical challenges described above, some conclusions can be reached about the reflectance of metals at 8 GPa, primarily from reverse configuration experiments.

For chromium, minor increases are observed in the infrared, but otherwise reflectance seems unchanged from its ambient condition. The reflectance of copper also appears to be unchanged from the ambient state. Platinum appears to become less reflective in the near-visible and mid-infrared region, but there evidence for a near-infrared decrease in some situations. For these three materials, there is no evidence of a strong reflectance increase, so assumptions that metal emissivity is close to its ambient value seem reasonable. As to whether emissivity increases or decreases from the ambient value, the evidence suggests that copper remains fixed, platinum increases somewhat, and chromium may decrease slightly. An important caveat to this interpretation is that most of the challenges mentioned above reduce the apparent reflectance of the sample, so this interpretation is preliminary at

[1] If target motion were important, one would expect continuous signal variations as the sample moved through the focal depth. Such variations were not observed.

present.

In the case of aluminum, two distinct outcomes were observed: no change in reflectance or consistent loss across all detector channels. The former is consistent with previous expectations, while the latter suggests a random geometric change, such as tilt. Calculations are underway to determine the tilt sensitivity of the optical relay to further study this issue.

5.4.3 Bond layer effects

In comparing standard and reverse configuration experiments, it becomes clear that the bonding layer plays a role the apparent reflectance of the compressed target. For example, minor near-infrared reflectance increases for reverse chromium targets become minor decreases in the standard configuration, indicating that the bond layer (AngstromBond, in this case) becomes slightly absorbing at 8 GPa. Strong near-visible absorption is also observed for both AngstromBond and Loctice 326. Mid-infrared absorption is also present at intermediate strength as shown in Figure 5.1 (NSLS07-12, Loctite 326 glue). In this example, the Si channel drops by 32%, the InGaAs channel by 7%, and the PEM channels by 13–16%. This drop does not correspond to an increasing sample emissivity, but would rather decrease the amount of sample emission that could be detected. Note that light in the reflectance measurement passes through the bond twice, whereas radiation emitted by the sample would only pass through the bond once.

Bond thickness is a key parameter in assessing absorption strength, and may explain why some standard metal reflectance experiments (NSLS06-14) show no reflectance changes while others do (NSLS06-19). However, precise measurements of the glue bond within a material stack have proven elusive. At present, the highest resolution obtained in this project is 0.002 mm. Bond thicknesses inferred by subtracting the window thicknesses from the total stack thickness yield positive and negative values within this uncertainty, so it is impossible to distinguish “thin” bond samples from “thick” bond samples when comparing different reflectance measurements. There is a fundamental weakness of the bond thickness measurement—maintaining nano-scale resolution over macroscopic parts—that must be overcome for precise characterization of epoxy absorption.

There is some evidence that the absorption of AngstromBond might be pressure dependent. In 5 GPa experiments (NSLS07-09 and NSLS07-10), there is noticeably less signal loss than in similar 8 GPa experiments (NSLS07-05 and NSLS07-08). Without precise bond thickness comparison, however, it is impossible to quantify this effect.

5.4.4 High emissivity coating

Reverse configuration experiments on the Sandia high emissivity coating largely show consistent reflectance losses on all detectors; one experiment indicated a slight rise on all channels. As in the case of aluminum, the consistent loss on all channels suggests a geometric reflectance change, and further study is needed to address this possibility. Standard re-

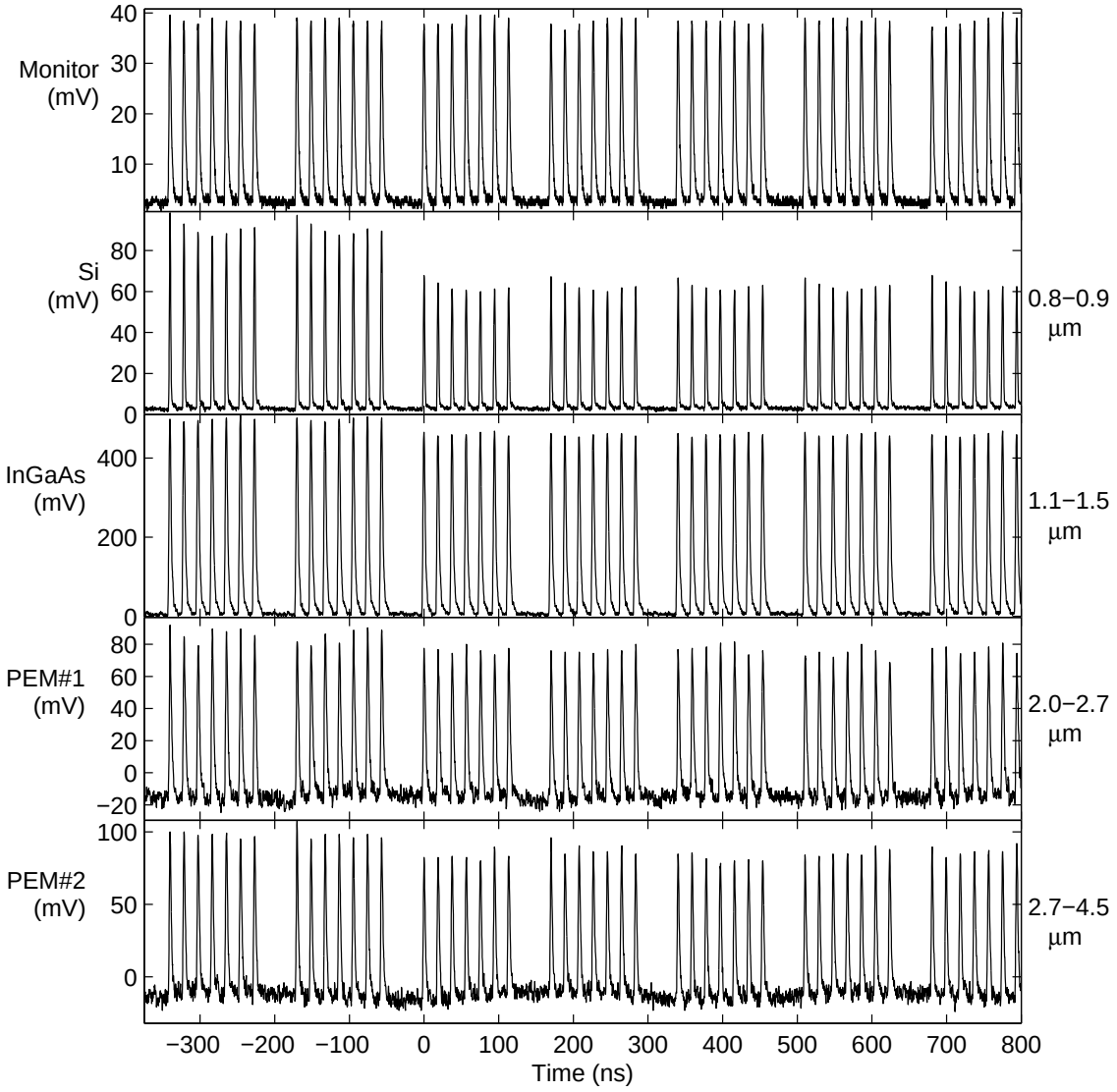

Figure 5.1. Bond layer absorption example (NSLS07-12, Loctite 326 glue)

flectance measurements of this film also show signal loss, though it is unclear how much of this is due to emissivity increase versus epoxy absorption. In any event, there is no evidence of catastrophic failure of the high emissivity film, *i.e.* the film does not be strongly reflective, so there is a strong possibility that it might serve as a useful emissivity standard.

It is important to note that the relative changes in the high emissivity film reflectance have a lower emissivity impact than in the metal samples. To illustrate this point, consider the reflectance of the compressed state to be some fraction of the ambient reflectance.

$$\rho = \rho_0 (1 + f) \tag{5.1}$$

The parameter f describes the amount by which reflectance changes in the compressed state. For an opaque sample, emissivity is the difference between unity and the reflectance.

$$\begin{aligned} \varepsilon &= 1 - \rho = 1 - \rho_0 - \rho_0 f \\ &= \varepsilon_0 - f\rho_0 \end{aligned} \tag{5.2}$$

Simply put, small fractional reflectance changes of a shiny surface (like a metal) correspond to larger emissivity variations than the same fractional change of a less reflective material. It is the relative gain or loss f that is probed in this work, so caution is needed when comparing results for different materials.

5.5 Data reduction

Given the poor noise performance of the mid-infrared detectors, some effort was made in reducing the measured signals into a more useful form. Essentially, this process exchanges time resolution for a smooth, consistent signal using the known properties of the VUV ring. Since the analysis is still under development, only a conceptual description and one example are presented.

5.5.1 Concept

Rather than dealing the instantaneous signal generated by the detector, it is useful to consider the number of photons emitted by the synchrotron during the passage of a single electron bunch. Assuming that the detector is sufficiently fast to recover between synchrotron pulses, the total number electrons striking the detector from a synchrotron pulse is proportional to the *area* under the detector pulse. By looking at pulse areas, rather than instantaneous pulse heights, it is possible to remove much of the high frequency noise present in the PEM detectors.

In this approach, precise details of the synchrotron can be used to constrain the integration domain locations. The VUV ring operates at a frequency 52.887 MHz, during which time nine electron "buckets" pass by each beam line. In standard operation, only seven of these buckets are filled, while the remaining two are left unoccupied. By cross correlating this bunch structure with a detector signal, it is possible to locate the best peak times about which to integrate the signal.

Setting the local integration domain width is ultimately based on the time response to the detector. If the detector rise and fall time is less than half the separation between synchrotron pulses, it is possible to break up the signal into a set of "on" and "off" pulses. "On" pulses are centered about the peak times described above, and extend 25% of the peak-peak time in either direction; "off" pulses are calculated between adjacent "on" pulses. The latter are useful in characterizing and removing background variations from the former, and also provide estimates of the signal-noise ratio. At this time,"off" pulse calculations and corrections have not been implemented into the data reduction code.

5.5.2 Example

Figure 5.2 shows reduced data from experiment NSLS07-12. For clarity, the curves have been normalized with signal obtained prior to shock compression. Certainly, the trends described in Section 5.4.3 are far more visible than in the raw signals (Figure 5.1). As expected, the Si and InGaAs detector results are much cleaner than the PEM results. Some improvements, such as inclusion of the "off" pulses, may reduce the PEM scatter further.

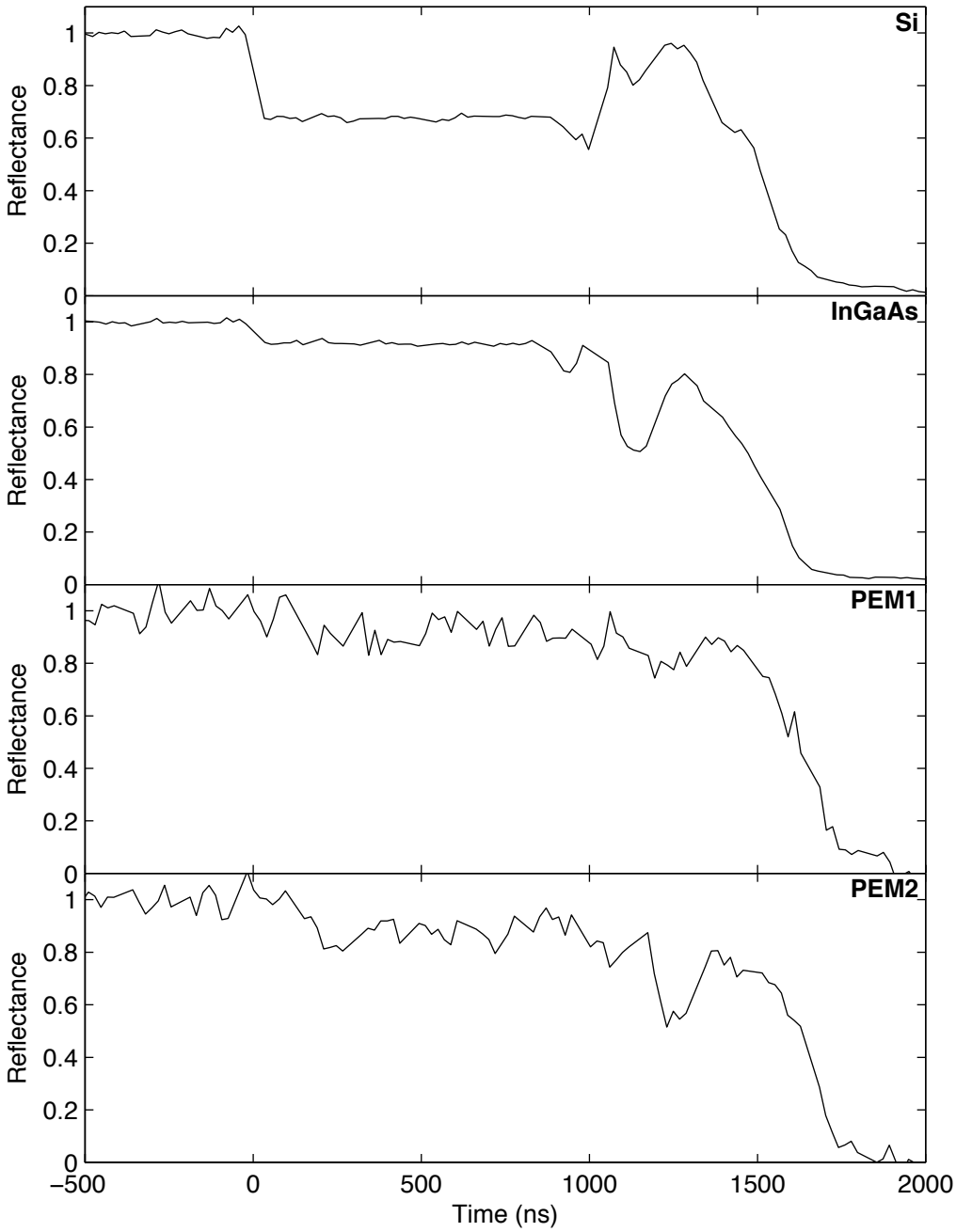

Figure 5.2. Data reduction example (NSLS07-12)

CHAPTER 6

Summary and future work

Over the three year course of this project, a platform was created for measuring infrared reflectance changes in shock compressed materials. Key achievements and suggestions for future work are summarized below.

6.1 Project summary

A primary object of this project was the integration of a gas gun system with a synchrotron. In doing so, broad band infrared reflectance measurements were performed on materials during shock compression. General project achievements include:

- Construction and validation of a 3" gas gun at Sandia.
- Installation of this gun at beam line U1 of the VUV ring at the National Synchrotron Light Source.
- Safe operation of the NSLS gas gun over three experiment campaigns (47 shots performed onsite).
- Construction of an optical relay to couple synchrotron light into and out of the gas gun target chamber for specular reflectance measurements.
- Demonstration of near- and mid-infrared measurements with single pulse resolution.

Dynamic reflectance measurements were performed on a variety of materials. In general, metal samples (Al, Cr, Cu, and Pt) maintained their ambient reflectance or became slightly less reflective (more emissive), an assumption common in most dynamic pyrometry research. For target configurations where light passes through a bonding layer, light is often absorbed in that layer, even when the bond is a few microns or less thick. In addition to metal films, a low reflectance Sandia coating was tested, showing promising behavior for its use as an emissivity standard. Reflectance geometry changes are an outstanding issue, so results indicating emissivity increase are preliminary at this time.

6.2 Recommendations for future work

Various technical challenges encountered in this project must be addressed for future infrared synchrotron studies of dynamically compressed materials. Limitations encountered in this project include:

- Impact velocity range.
- Low signal levels confined to broad spectral measurements, particularly for low reflectance samples.
- Potential sensitivity to minor geometric reflectance changes.
- Characterization and control of bond thickness.
- Distinguishing sample reflectance changes from bond layer transparency loss.

Several of these challenges are being addressed in a followup collaboration with Los Alamos National Laboratory. New gas gun systems, capable of generating impact velocities up to 1 km/s, are already under construction. A gated infrared spectrometer for measuring continuous spectra over one synchrotron orbit is under development in collaboration with National Security Technologies to expand spectroscopic capabilities. Revised optical relay systems are also under development to handle geometric reflectance changes (tilt or diffuse related) at National Security Technologies. As part of these developments, more rigorous timing practices [16] will be implemented to synchronize advanced diagnostics with the synchrotron and impact event.

Characterization and control of the bond layer thickness is a area where improvements are needed. Currently, the bond layer thickness is nearly equal to the measurement precision (0.002 mm), making quantitative comparison bond absorption impossible. In this thickness domain, interference effects clearly play a role, but the extent to which such interference changes during compression is not know. Because of these problems, it would seem that the reverse configuration is best suited for reflectance and pyrometry studies, though bond thickness remains important in thermal conduction. An epoxy free configuration proposed by Urtiew and Grover [12], may be useful in future studies, especially when combined with the high emissivity film.

In the long term, infrared synchrotron studies of dynamically compressed materials will require additional infrastructure. For reasons of safety and debris containment, an enclosed space near a synchrotron port would be highly advantageous. Dynamic compression users often need direct optical and/or x-ray port access for broadband measurements, not standard end station equipment (*e.g.*, FTIR spectrometers). A more permanent presence at NSLS, along with plans to integrate with NSLS II, is needed to bring more dynamic compression users to these unique facilities.

References

[1] Barker, L. and Hollenbach, R. Laser interferometer for measuring high velocities of any reflecting surface. *Journal of Applied Physics* **43**, 4669 (1972).

[2] Plank, M. On the law of distribution of energy in the normal spectrum. *Annalen der Physik* **4**, 553 (1901).

[3] DeWitt, D. and Nutter, G., editors. *Theory and Practice of Radiation Thermometry*. Wiley, New York, (1988).

[4] Palik, E., editor. *Handbood of Optical Constants of Solids*. Academic Press, (1985).

[5] Partouche-Sebban, D., Holtkamp, D., Pelissier, J., Taboury, J., and Rouyer, A. An investigation of shock induced temperature rise and melting of bismuth using high-speed optical pyrometry. *Shock Waves* **11**, 385–392 (2002).

[6] Partouche-Sebban, D. and Pelissier, J. Emissivity and temperature measurements under shock loading along the melting curve of bismuth. *Shock Waves* **13**, 69–81 (2003).

[7] Poulsen, P. and Ault, S. New method of high-precision thermometry. *Review of Scientific Instruments* **77**, 94901 (2006).

[8] Duvall, G. and Graham, R. Phase transitions under shock wave loading. *Reviews of Modern Physics* **49**(3), 523 (1977).

[9] Fowles, G., Duvall, G., Asay, J., Bellamy, P., Feistmann, F., Grady, D., Michaels, T., and Mitchell, R. Gas gun for impact studies. *Review of Scientific Instruments* **41**(7), 984–996 (1970).

[10] Fat'yanov, O., Webb, R., and Gupta, Y. Optical transmission through inelastic deformed shocked sapphire: stress and crystal orientation effects. *Journal of Applied Physics* **97**, 123529 (2005).

[11] Partouche-Sebban, D., Pelissier, J., Abeyta, F., Anderson, W., Byers, M., Dennis-Koller, D., Esparza, J., Hixson, R., Holtkamp, D., Jensen, B., King, J., Rigg, P., Rodriguez, P., Shampine, D., Stone, J., Westley, D., Borror, S., and Kruschwitz, C. Measurement of the shock-heated melt curve of lead using pyrometry and reflectometry. *Journal of Applied Physics* **97**, 43521 (2005).

[12] Urtiew, P. and Grover, R. Temperature deposition caused by shock interactions with material interfaces. *Journal of Applied Physics* **45**(1), 140 (1974).

[13] Bergstresser, T. and Becker, S. Temperature measurement of isentropically accelerated flyer plates. In *Shock Compression of Condensed Matter,* Furnish, M., editor, volume 620, 1169, (2001).

[14] Dereniak, E. and Boreman, G. *Infrared Detectors and Systems*. John Wiley & Sons, (1996).

[15] Lemke, R., Knudson, M., Bliss, D., Cochrane, K., Davis, J.-P., Giunta, A., Harjes, H., and Slutz, S. Magnetically accelerated, ultrahigh velocity flyer plates for shock wave experiments. *Journal of Applied Physics* **98**, 73530 (2005).

[16] Rigg, P. *Real-time x-ray diffraction to examine lattice deformation in shocked lithium fluoride windows*. PhD thesis, Washington State University, (1999).

DISTRIBUTION:

2 Steve Becker
Bechtel Nevada
Las Vegas Operations
PO Box 98521
Las Vegas, NV 89193

2 Chris Deeney
Office of Defense Science, NA-113
National Nuclear Security Administration
U.S. Dept. of Energy
1000 Independence Ave.
Washington, DC 20585

2 Y.M. Gupta
Institute for Shock Physics
Washington State University
Pullman, WA 99164-2816

2 R.J. Hemley
Carnegie DOE Alliance Center
5251 Broad Branch Road, NW
Washington DC 20015-1305

2 Chi-Chang Kao
National Synchrotron Light Source
Brookhaven National Laboratory
P.O. Box 5000, Bldg. 725B
Upton, NY 11973-5000

2 David Holtkamp
Los Alamos National Laboratory
P.O. Box 1663
Los Alamos, NM 87545

2 Brian Jensen
Los Alamos National Laboratory
P.O. Box 1663
Los Alamos, NM 87545

2 M.F. Nicol
UNLV High Pressure Sciences and Engineering Center
University of Nevada, Las Vegas
Box 454002
4505 South Maryland Parkway
Las Vegas, NV 89154-4002

2 Gerald Stevens
Bechtel Nevada
Special Technologies Laboratory
5520 “B” Ekwill Street
Santa Barbara, CA 93111

2 Mark Wilke
Los Alamos National Laboratory
P.O. Box 1663
Los Alamos, NM 87545

1	MS	1181	S.C. Alexander, 1647
1	MS	1181	T. Ao, 1646
1	MS	1181	J.R. Asay, 1646
1	MS	1181	J.-P. Davis, 1646
5	MS	1181	D.H. Dolan, 1646
1	MS	1181	M.D. Furnish, 1647
2	MS	1181	C.A. Hall, 1646
1	MS	1181	R.J. Hickman, 1646
1	MS	1152	M.L. Keifer, 1652
1	MS	1181	M.D. Knudson, 1646
2	MS	1181	T. Mehlhorn, 1640
1	MS	1181	W.D. Reinhart, 1647
1	MS	1181	M.D. Roderick, 1646
1	MS	1181	T.J. Vogler, 1647
1	MS	1181	J. Wise, 1646
1	MS	9018	Central Technical Files, 8944 (electronic copy)
1	MS	0899	Technical Library, 9536 (electronic copy)
1	MS	0123	D. Chavez, LDRD Office, 1011